Asymmetric Thin-Shell Wormhole

Seyed Danial Forghani

Submitted to the
Institute of Graduate Studies and Research
in partial fulfillment of the requirements for the degree of

Doctor of Philosophy
in
Physics

Eastern Mediterranean University
September 2019
Gazimağusa, North Cyprus

Approval of the Institute of Graduate Studies and Research

Prof. Dr. Ali Hakan Ulusoy
Acting Director

I certify that this thesis satisfies all the requirements as a thesis for the degree of Doctor of Philosophy in Physics.

Prof. Dr. İzzet Sakallı
Chair, Department of Physics

We certify that we have read this thesis and that in our opinion it is fully adequate in scope and quality as a thesis for the degree of Doctor of Philosophy in Physics.

Prof. Dr. Mustafa Halilsoy
Co-Supervisor

Prof. Dr. S. Habib Mazharimousavi
Supervisor

Examining Committee

1. Prof. Dr. Muzaffer Adak
2. Prof. Dr. Özay Gürtuğ
3. Prof. Dr. S. Habib Mazharimousavi
4. Prof. Dr. Omar Mustafa
5. Prof. Dr. İzzet Sakallı

ABSTRACT

Wormholes appeared in general relativity as special solutions to Einstein's field equations. These bizarre structures can be visualized as tunnels connecting remote points within a single spacetime or points of two distinct spacetimes. The main problem with the wormholes is that they are supported by exotic matter; a kind of matter which does not satisfy the known energy conditions. In 1988, Morris and Thorne published a paper and discussed the traversability of wormholes. The paper soon came to researchers' focus and caused a new wave of studies over structural characteristics of wormholes. In 1989, in one of these attempts, Visser developed a method with which a new class of traversable wormholes came into existence; *thin-shell wormholes*. The principal aim was to tackle with the exotic matter that necessarily gave life to such objects. Visser's recipe was to confine the exotic matter to a very narrow surface, i.e. the throat of the thin-shell wormhole so that its existence can be justified in some way. Thin-shell wormholes in isotropic spacetimes are represented traditionally by embedding diagrams which were symmetric paraboloids. This mirror symmetry, however, can be broken by considering different sources on different sides of the throat. This gives rise to an *asymmetric thin-shell wormhole*, whose mechanical stability is studied here in the framework of the linear stability analysis. In the first half of this dissertation, having constructed a general formulation, using barotropic and variable equations of state, also related junction conditions, the results are closely studied for some examples of diverse geometries in general relativity. Specifically, the role of asymmetry in the stability of thin-shell wormholes, if any, has been studied. It is shown that the stability of such peculiar objects can be studied in the context of linear stability analysis and that they can

be mechanically stable. It is seen that the asymmetric structures of thin-shell wormholes are less likely to be stable compared with their symmetric counterparts. Also, it is shown that the discontinuities which appear in the stability diagrams of the asymmetric thin-shell wormholes are due to a flaw in the barotropic equation of state, and that such discontinuities can be lifted by exploiting a radius-dependent variable equation of state. The second half is devoted to constructing static thin-shell wormholes in new massive gravity and investigating their properties. It is shown that the asymmetry arises naturally in these thin-shell wormholes. Additionally, solutions such as static BTZ and new type black holes, and warped (A)dS$_3$ solutions admit no thin-shell wormholes. Finally, the energy density and pressure of the constructed asymmetric thin-shell wormholes become zero which implies no exotic matter.

Keywords: Thin-Shell Wormhole, Thin-Shell Formalism, General Relativity, New Massive Gravity, Exotic Matter, Asymmetry.

ÖZ

Genel görelilikte solucan delikleri, Einstein'ın alan denklemlerine özel çözümler olarak ortaya çıktı. Bu tuhaf yapılar, tek bir uzay-zaman içindeki uzak noktaları veya iki farklı uzay-zamanın noktalarını birbirine bağlayan tüneller olarak tasavvur edilebilir. Solucan delikleri ile ilgili ana problem, fiziksel olmayan madde -bilinen enerji koşullarını sağlamayan bir tür madde- ile desteklenmeleridir. 1988'de, Morris ve Thorne bir makale yayınladı ve solucan deliklerinin geçilebilirliğini tartıştı. Makale kısa sürede araştırmacıların odağı haline geldi ve solucan deliklerinin yapısal özellikleri üzerinde yeni bir çalışma dalgası yarattı. 1989'da, bu girişimlerden birinde, Visser, yeni bir geçilebilir solucan deliği sınıfının ortaya çıktığı bir yöntem geliştirdi; ince-kabuklu solucan delikleri. Asıl amaç, bu tür nesnelere zorunlu olarak hayat veren fiziksel olmayan madde ile baş etmekti. Visser'in çözümü, fiziksel olmayan maddeyi çok dar bir yüzeye, yani ince-kabuklu solucan deliğinin boğazına sınırlamaktı ki böylece varlığı bir şekilde doğrulanabilirdi. İzotropik uzay-zamanlarda ince-kabuklu solucan delikleri, geleneksel olarak bakışımlı paraboloitler olan diyagramların yerleştirilmesiyle gösterilir. Ancak bu ayna bakışımlılığı, boğazın çeşitli taraflarında başka kaynaklar göz önünde bulundurularak kırılabilir. Bu da, lineer kararlılık analizi çerçevesinde mekanik kararlılığı burada incelenmiş olan bakışımsız bir ince-kabuklu solucan deliğini ortaya çıkartır. Bu tezin ilk yarısında, barotropik ve değişken durum denklemleri ve ayrıca ilgili birleşme koşulları da kullanılarak genel bir formülasyon elde edilerek, sonuçlar genel görelilikteki farklı geometrilerin bazı örnekleri için yakından incelenmiştir. Spesifik olarak, ince-kabuklu solucan deliklerinin kararlılığında bakışımsızlığın rolü, eğer varsa, incelenmiştir. Lineer kararlılık analizi bağlamında, böyle tuhaf nes-

nelerin kararlılığının çalışılabileceği ve mekanik olarak kararlı olabilecekleri gösterilmiştir. İnce-kabuklu solucan deliklerinin bakışımsız yapılarının, bakışımlı benzerlerine kıyasla daha az kararlı oldukları görülmüştür. Ayrıca, bakışımlı ince-kabuklu solucan deliklerinin kararlılık diyagramlarında görünen süreksizliklerin, barotropik durum denklemindeki bir kusurdan kaynaklandığı ve bu tür süreksizliklerin yarıçap-bağımlı değişken durum denkleminden yararlanılarak kaldırılabileceği gösterilmiştir. İkinci yarı, yeni kütleli çekim kuramında statik ince-kabuklu solucan delikleri elde etmeye ve bunların özelliklerini araştırmaya adanmıştır. Bu ince-kabuklu solucan deliklerinde bakışımsızlığın doğal olarak ortaya çıktığı gösterilmiştir. Ek olarak, statik BTZ ve yeni tip kara delikler gibi çözümler ve eğrilmiş (A)dS3 çözümleri, ince-kabuklu solucan deliklerini desteklememektedir. Son olarak, elde edilen bakışımsız ince-kabuklu solucan deliklerinde enerji yoğunluğu ve basınç sıfır olmakta ve bu da fiziksel olmayan madde olmadığı anlamına gelmektedir.

Anahtar Kelimeler: İnce-kabuklu solucan deliği, İnce-kabuk forrmalizmi, Genel görelilik, Yeni kütleli çekim kuramı, Fiziksel olmayan madde, Bakışımsızlık.

To my extraordinary family

for their support and encouragement

ACKNOWLEDGMENT

Throughout my graduate program and the writing of this dissertation I received a great deal of support and assistance. I would first like to thank my dear supervisor and co-supervisor, Prof. Dr. S. Habib Mazharimousavi and Prof. Dr. Mustafa Halilsoy, whose expertise, wisdom and diligence lit up all the way from the first day to the last. It would simply be impossible to make it without you.

I would like to kindly thank our department's staff members. Specially, I would like to single out our chair of department, Prof. Dr. İzzet Sakallı, for all the opportunities that I have been given. It has been a privilege to work under your chairmanship. I would also like to express my deepest gratitude to my dear professors, Prof. Dr. Omar Mustafa and Prof. Dr. Özay Gürtuğ, and our department's chair of graduate studies, Assist. Prof. Dr. Mustafa Rıza, for their valuable guidance. You provided me with the tools that I needed to choose the right direction and successfully complete my Ph.D. program. Special thanks to our dear Secretary, Mrs. Çilem Aydınlık and our lab technician, Mr. Reşat Akoğlu for all the kindness and pleasantness they have always been offering.

I would also like to acknowledge my current and former colleagues, Sara Kanzi, Gülnihal Tokgöz, Huriye Gürsel, Niloufar Abtahi, Ali Övgün, Yashar Alizadeh, Morteza Kerachian, Zeinab Alghadi, Masoumeh Izadparast and Yashmitha Kumaran. You were of great support in deliberating over our problems and findings, as well as providing happy distraction to rest my mind outside of my research.

Last but not least, I am the most grateful of my family, my parents, my brothers, Davood and Dara, My grandparents, my uncles Roozbeh and Mehdi, and my dear fiancé, Mobina, for all the unconditional love and support. Thank you for always being there for me.

TABLE OF CONTENTS

LIST OF FIGURES

Chapter 1

INTRODUCTION

The history of wormholes goes back to the embedding diagrams of Ludwig Flamm [1] in the newly discovered Schwarzschild metric in 1916. Later on, in 1935, Einstein and Rosen [2] in search of a geometric model for elementary particles rediscovered a wormhole as a tunnel connecting two asymptotically flat spacetimes. The minimum radius of the tunnel, now known as the throat connecting two geometries, was interpreted as the radius of an elementary particle. The idea of wormhole did not go in much popularity until Morris and Thorne [3,4] gave a detailed analysis, and in certain sense, initiated the modern age of wormholes as tunnels connecting two spacetimes. It was already stated by Morris and Thorne that the energy density of such an object, if it ever exists, must be negative; a notorious concept in the realm of classical physics. This could be supported by a type of hypothetical matter known as the exotic matter. Exotic matter, which inevitably emerges in the theories of wormholes, violates the known energy conditions such as the weak energy condition (WEC) [5]. In fact, wormholes in general relativity violate all of the pointwise and averaged energy conditions [4, 6]. In quantum theory, rooms exist to manipulate and live along peacefully with negative energy densities. However, being a classical theory, general relativity must find the remedy within its classical regime without resorting to any quantum physics. At this stage, an important contribution came from a new chapter in wormhole theories; thin-shell wormhole (TSW). The concept of TSW was introduced by Visser in 1989 [7, 8]

in the hope of keeping the idea of wormholes alive by confining the exotic matter to a narrow band of the spacetime, called the throat of the TSW. The idea of TSWs became as popular and interesting as the standard wormholes, verified extensively by the literature in that context [9–39]. Prior to Visser's articles, wormhole theories had the exotic matter distributed on certain parts of the spacetime, if not all over it. However, Visser's so called cut-and-paste procedure allows us to confine such a notorious matter on a very limited part of the space, the TSW itself. Moreover, the cut-and-paste procedure has the advantage that can be applied to a vast variety of spacetimes [21–33], while before Visser only some certain spacetimes had the structure of a wormhole [6]. It is also worth mentioning that while TSWs are categorized as traversable wormholes, not all the wormholes are considered to be traversable [3]. As another advantage in favor of TSWs, Poisson and Visser developed a method [10] with which the dynamical stability of TSWs could be appraised under a radial perturbation [32–39]. For some more recent works we refer to [40–76]. Let us also remark that there have been attempts to construct TSWs with total positive energy against the negative local energy density [77–83]. This has been possible only by changing the geometrical structure of the throat, namely from spherical/circular to non-spherical/non-circular geometry, depending on the dimensionality. Stability of TSW is another important issue that deserves mentioning and investigation for the survival of a wormhole (Fig. 1) [27–31, 34, 35, 45, 46, 84–86].

In this dissertation, we introduce TSWs that are constructed asymmetrically out of different bulk spacetimes [87–90]. So far, the spacetimes on the two sides of the throat have been made from the same bulk material. Our intention is to consider different spacetimes, or at least different sources in common types of spacetimes to impose a

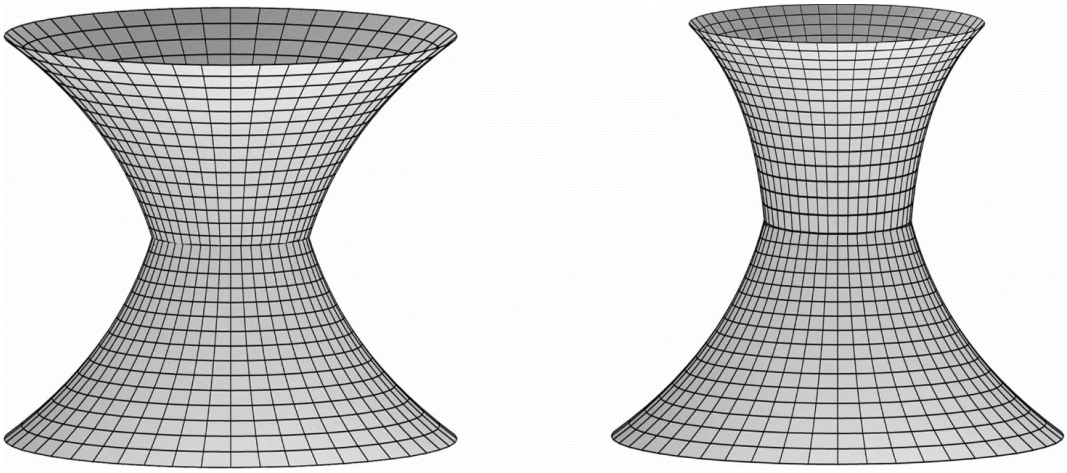

Figure 1.1: Schematic embedding diagram of a symmetric (left) and an asymmetric (right) thin-shell wormhole.

difference between the two sides. Naturally, the reflection symmetry about the throat in the upper and lower halves will be broken and in consequence new features are expected to arise which is the basic motivation for the present study. Note that for non-isotropic bulks, asymmetric TSWs emerge naturally. For example, we consider Reissner–Nordström (RN) spacetimes on both sides of the throat, but with different masses and/or charges; Or two cosmic string (CS) spacetimes with different deficit angles. This type of TSW, which we dub as asymmetric TSW (ATSW), has not been investigated so far and so we will be focusing on them. One may anticipate that the asymmetry of the wormhole will have an impact on particle geodesics, light lensing, and other matters. Asymmetry may act instrumental in the identification of TSWs in nature, if there exists such structures. Our next concern will be to study the stability of such ATSWs and novelties that may arise, if any. As in the previous studies, an equation of state (EoS) is introduced at the throat with pressure and density to be used as the surface energy-momentum tensor. Then, the Darmois-Israel junction conditions [92–97] relate these variables within an energy equation. Next is to radially perturb the ATSW to see how this energy equation responds to the perturbation. Based

on the response, which is studied within the linear stability analysis framework, the stability of the ATSW is assessed. In chapter 2, we study ATSWs in general relativity constructed by, first, spherically symmetric and then, cylindrically symmetric solutions of Einstein's equations. Furthermore, we address an anomaly which occasionally occurs in the stability diagram of an ATSW, called the infinite discontinuity. We discuss what gives rise to it and how it can be removed. In chapter 3, static ATSWs are constructed in new massive gravity. There we reveal that for possible ATSW constructions, exotic matter is not required. We conclude in chapter 4. Throughout the manuscript, we follow the unit convention $c = 8\pi G_{(n+1)} = 4\pi\varepsilon_{0(n+1)} = 1$, where c is the speed of light, and $G_{(n+1)}$ and $\varepsilon_{0(n+1)}$ are the gravitational constant and the permittivity of free space in $n+1$ dimensions, respectively. Moreover, to improve the readability of the manuscript, we use the unusual term "*side-spacetimes*" to refer to the two bulk spacetimes on the two sides of the throat of an ATSW.

Chapter 2

ASYMMETRIC THIN-SHELL WORMHOLES IN GENERAL RELATIVITY

2.1 Construction of a Spherical ATSW

To study the ATSWs in general relativity, we begin by specifying to the two side-spacetimes, two general $3+1$-dimensional spherically symmetric line elements in spherical coordinates $x_{\pm}^{\mu}=\{t_{\pm},r_{\pm},\theta_{\pm},\phi_{\pm}\}$, given by

$$ds_{\pm}^{2}=g_{\mu\nu}^{\pm}dx_{\pm}^{\mu}dx_{\pm}^{\nu}=-A_{\pm}(r_{\pm})\,dt_{\pm}^{2}+B_{\pm}(r_{\pm})\,dr_{\pm}^{2}+C_{\pm}(r_{\pm})\,d\Omega_{\pm}^{2}, \qquad (2.1)$$

in which, $g_{\mu\nu}^{\pm}$ are the metric tensors of the two sides. The metric functions $A_{\pm}(r_{\pm})$, $B_{\pm}(r_{\pm})$ and $C_{\pm}(r_{\pm})$ are all positive functions of radial coordinates $r_{\pm}$, whereas $d\Omega_{\pm}^{2}$, traditionally, are $2-$sphere line elements defined by $d\Omega_{\pm}^{2}=d\theta_{\pm}^{2}+\sin^{2}\theta_{\pm}d\varphi_{\pm}^{2}$.

To construct an ATSW, following the Visser's method in the spherical coordinates, consider two distinct Lorentzian spacetimes denoted by $(\Sigma,g)^{\pm}$, each having a line element of the form in Eq. (2.1). Out of each spacetime, a subset $(\Upsilon,g)^{\pm}$ is cut such that no singularities or event horizons of any sort are included, i.e. $(\Upsilon,g)^{\pm}\subset(\Sigma,g)^{\pm}$ and $(\Upsilon,g)^{\pm}=\{x_{\pm}^{\mu}|r_{\pm}\geq a(\tau)>r_{eh}\}$, where r_{eh} is any existed event horizon, and τ is the proper time on the shell $r_{\pm}=a$. Then, by pasting these two cuts at their common timelike hypersurface $\mathcal{H}$, such that $\mathcal{H}\subset(\Upsilon,g)^{\pm}$, one creates a geodesically complete Riemannian spacetime which provides a passage from one spacetime to the other. The

whole structure is called, in general, an ATSW, and the hypersurface $\mathcal{H}$ is indeed the throat of the ATSW which contains the exotic matter. Note that, the coordinates of the two sides of the throat $x_{\pm}^{\mu}$, and more generally, the very natures of the two spacetimes do not necessarily need to be the same. However, if they are chosen to be exactly the same, the ATSW reduces to an ordinary symmetric TSW. To analyze the stability of the throat, one spots the time-dependent throat characterized by $r_{\pm} = a(\tau)$, or implicitly

$$\mathcal{H}(r_{\pm}, \tau) = r_{\pm} - a(\tau) = 0, \tag{2.2}$$

where τ is the proper time measured by the observer on the shell. In the context of Darmois-Israel junction formalism [91–97], two conditions must be satisfied at the TSW's throat. While the first junction condition expects a continuity in the first fundamental form, the second one requires a discontinuity in the second fundamental form of the throat. Accordingly, the first junction condition gives rise to a unique line element on the shell given by

$$ds_{\mathcal{H}}^2 = h_{ab} d\xi^a d\xi^b = -d\tau^2 + C(a(\tau))\, d\Omega^2, \tag{2.3}$$

no matter from which spacetime one approaches the throat. Herein, $\xi^a = \{\tau, \theta, \phi\}$ are the coordinates and h_{ab} are the components of the metric tensor on the throat. Equating Eqs. (2.1) and (2.3) at the location of the throat, $r_{\pm} = a(\tau)$, immediately results in

$$\left[-A_{\pm}(r_{\pm})\, dt_{\pm}^2 + B_{\pm}(r_{\pm})\, dr_{\pm}^2\right]_{r_{\pm}=a(\tau)} = -d\tau^2, \tag{2.4a}$$

$$C_{\pm}(r_{\pm})\big|_{r_{\pm}=a(\tau)} = C(a(\tau)), \tag{2.4b}$$

and

$$\{\theta_{\pm}, \phi_{\pm}\} = \{\theta, \phi\}. \tag{2.4c}$$

The first equation of the set above (Eq. (2.4a)), gives rise to an expression for the square of the total derivative of $t_\pm$ with respect to the proper time τ, denoted by an overdot as

$$\dot{t}_\pm^2 = \frac{1 + B_\pm \dot{a}^2}{A_\pm}. \tag{2.5a}$$

Also, by taking derivative with respect to the proper time τ of the two sides of the equation above, one calculates

$$\ddot{t}_\pm = \frac{\dot{a}\left(A_\pm B'_\pm \dot{a}^2 - A'_\pm B_\pm \dot{a}^2 + 2A_\pm B_\pm \ddot{a} - A'_\pm\right)}{2A_\pm^{3/2}\sqrt{(1 + B_\pm \dot{a}^2)}}. \tag{2.5b}$$

These two latter expressions will be used later in the calculations of the second junction condition which leads to the components of the second fundamental form. Furthermore, Eq. (2.4b) states that the metric functions $C_\pm(r_\pm)$ must be equal at any given proper time τ at the location of the throat. This places a strong condition over these metric function, imposing that the two functions $C_\pm(r_\pm)$ must have a similar radial-dependent structure, i.e. we must have $C_+(r_+) = C_-(r_-)$ at any given time τ. The second junction condition is mathematically given by [93]

$$[K_b^a]_-^+ - \delta_b^a [K]_-^+ = -S_b^a, \tag{2.6}$$

where K_b^a, K, and S_b^a indicate the mixed extrinsic curvature tensor, the total curvature, and the energy-momentum tensor of the throat, respectively. Also, δ_b^a is the Kronecker delta, and the square brackets $[\,]_-^+$ impart a jump in the included physical quantity passing across the throat, i.e. $[\Upsilon]_-^+ = \Upsilon_+ - \Upsilon_-$. The standard definition of the covariant extrinsic curvature of the throat is given by

$$K_{ab}^\pm = -n_\mu^\pm \left(\frac{\partial x_\pm^\mu}{\partial \xi^a \partial \xi^b} + \Gamma_{\alpha\beta}^{\mu\pm} \frac{\partial x_\pm^\alpha}{\partial \xi^a} \frac{\partial x_\pm^\beta}{\partial \xi^b} \right), \tag{2.7}$$

where

$$n_{\mu}^{\pm}=\left(g_{\pm}^{\alpha\beta}\frac{\partial\mathcal{H}}{\partial x_{\pm}^{\alpha}}\frac{\partial\mathcal{H}}{\partial x_{\pm}^{\beta}}\right)^{-1/2}\frac{\partial\mathcal{H}}{\partial x_{\pm}^{\mu}} \tag{2.8}$$

are the spacelike four-normal vectors at the location of the throat satisfying $n_{\mu}^{\pm}n_{\pm}^{\mu}=+1$ for the timelike hypersurface, while

$$\Gamma_{\alpha\beta}^{\mu\pm}=\frac{1}{2}g_{\pm}^{\mu\nu}\left(\frac{\partial g_{\alpha\nu}^{\pm}}{\partial x_{\pm}^{\beta}}+\frac{\partial g_{\nu\beta}^{\pm}}{\partial x_{\pm}^{\alpha}}-\frac{\partial g_{\alpha\beta}^{\pm}}{\partial x_{\pm}^{\nu}}\right) \tag{2.9}$$

are the Christoffel symbols of the bulk geometries, compatible with $g_{\mu\nu}^{\pm}$. Note that, the Christoffel symbols for a torsion-free spacetime, such as the ones we consider here, are symmetric with respect to the commutation of their covariant indices [98]. This, in turn, gives that the extrinsic curvature tensor is a symmetric tensor under the commutation of its indices. To derive the explicit expressions for the second junction condition, let us start by calculating the unit vector components $n_{\mu}^{\pm}$. Having the defining equation of the hypersurface in Eq. (2.2), we find

$$\frac{\partial\mathcal{H}}{\partial t_{\pm}}=-\frac{\dot{a}}{\dot{t}_{\pm}}, \tag{2.10a}$$

$$\frac{\partial\mathcal{H}}{\partial r_{\pm}}=1, \tag{2.10b}$$

and

$$\frac{\partial\mathcal{H}}{\partial\theta_{\pm}}=\frac{\partial\mathcal{H}}{\partial\phi_{\pm}}=0. \tag{2.10c}$$

These equations, along with

$$g_{\pm}^{\alpha\beta}=diag\left(-A_{\pm}^{-1}\left(r_{\pm}\right),B_{\pm}^{-1}\left(r_{\pm}\right),C_{\pm}^{-1}\left(r_{\pm}\right),C_{\pm}^{-1}\left(r_{\pm}\right)\sin^{-2}\theta_{\pm}\right), \tag{2.11}$$

enable us to calculate

$$n_\mu^\pm = \left(-\dot{a}\sqrt{A_\pm B_\pm}, \sqrt{B_\pm\,(1+B_\pm \dot{a}^2)}, 0, 0 \right). \tag{2.12}$$

To find the components of the second fundamental form in Eq. (2.7), one also needs to compute for the Christoffel symbols given by Eq. (2.9) [98]. With some algebra, the non-zero components of the Christoffel symbols are obtained as

$$\Gamma^{t\pm}_{tr} = \Gamma^{t\pm}_{rt} = \frac{A'_\pm}{2A_\pm}, \tag{2.13a}$$

$$\Gamma^{r\pm}_{tt} = \frac{A'_\pm}{2B_\pm}, \tag{2.13b}$$

$$\Gamma^{r\pm}_{tr} = \Gamma^{r\pm}_{rt} = \frac{B'_\pm}{2B_\pm}, \tag{2.13c}$$

$$\Gamma^{r\pm}_{\theta\theta} = -\frac{C'_\pm}{2B_\pm}, \tag{2.13d}$$

$$\Gamma^{r\pm}_{\phi\phi} = -\frac{C'_\pm \sin^2\theta_\pm}{2B_\pm}, \tag{2.13e}$$

$$\Gamma^{\theta\pm}_{r\theta} = \Gamma^{\theta\pm}_{\theta r} = \frac{C'_\pm}{2C_\pm}, \tag{2.13f}$$

$$\Gamma^{\theta\pm}_{\phi\phi} = -\sin\theta_\pm \cos\theta_\pm, \tag{2.13g}$$

$$\Gamma^{\phi\pm}_{r\phi} = \Gamma^{\phi\pm}_{\phi r} = \frac{C'_\pm}{2C_\pm}, \tag{2.13h}$$

and

$$\Gamma^{\phi\pm}_{\theta\phi} = \Gamma^{\phi\pm}_{\phi\theta} = \frac{\cos\theta_\pm}{\sin\theta_\pm}, \tag{2.13i}$$

where a prime $(')$ stands for a total derivative with respect to the radial coordinate r.

Collecting the results in Eqs. (2.5a, 2.5b), (2.12), and (2.13a-2.13i) into Eq. (2.7), one calculates the non-zero components of the mixed extrinsic curvature tensor as

$$K^{\tau}_{\tau\pm} = \sqrt{\frac{B_{\pm}}{1+B_{\pm}\dot{a}^2}}\left[\ddot{a} + \frac{A'_{\pm}}{2A_{\pm}B_{\pm}} + \frac{\dot{a}^2}{2}\left(\frac{A'_{\pm}}{A_{\pm}} + \frac{B'_{\pm}}{B_{\pm}}\right)\right] \tag{2.14a}$$

and

$$K^{\theta}_{\theta\pm} = K^{\phi}_{\phi\pm} = \sqrt{\frac{B_{\pm}}{1+B_{\pm}\dot{a}^2}}\left[\frac{C'_{\pm}}{2B_{\pm}C_{\pm}} + \frac{\dot{a}^2}{2}\left(\frac{C'_{\pm}}{C_{\pm}}\right)\right]. \tag{2.14b}$$

Note that, in these last equations one of the indices has been raised up by $K^{a}_{b\pm} = h^{ac}K^{\pm}_{bc}$. The total curvature $K_{\pm}$ is defined as the trace of the mixed extrinsic curvature tensor, i.e. $K_{\pm} \equiv Tr\left[K^{a}_{b\pm}\right] = h^{ab}K^{\pm}_{ab}$. Therefore, one obtains the total curvature as

$$K_{\pm} = K^{\tau}_{\tau\pm} + K^{\theta}_{\theta\pm} + K^{\phi}_{\phi\pm} = \sqrt{\frac{B_{\pm}}{1+B_{\pm}\dot{a}^2}}\times \left[\ddot{a} + \frac{1}{2B_{\pm}}\left(\frac{A'_{\pm}}{A_{\pm}} + 2\frac{C'_{\pm}}{C_{\pm}}\right) + \frac{\dot{a}^2}{2}\left(\frac{A'_{\pm}}{A_{\pm}} + \frac{B'_{\pm}}{B_{\pm}} + 2\frac{C'_{\pm}}{C_{\pm}}\right)\right]. \tag{2.15}$$

Having the non-zero components of the extrinsic curvature tensor and the total curvature, all one needs to finalize the second junction condition in Eq. (2.6), is to write down the components of the energy-momentum tensor S^{a}_{b}. In this regard, we assume that the exotic matter on the throat is a perfect fluid whose energy-momentum tensor is given by

$$S^{a}_{b} = diag(-\sigma, p, p). \tag{2.16}$$

Herein, σ is the energy density of the fluid on the throat and p is its angular/tangential pressure. Combining Eqs. (2.14a, 2.14b) and (2.15), together with the energy-momentum tensor of the shell in Eq. (2.16), turns the second Darmois-Israel junction conditions

in Eq. (2.6) into the following set of equations:

$$\sigma = -\frac{C'}{C}\sum_{i=+,-}\sqrt{\frac{1+B_i\dot{a}^2}{B_i}} \tag{2.17a}$$

and

$$p = \sum_{i=+,-}\left\{\sqrt{\frac{B_i}{1+B_i\dot{a}^2}}\left[\ddot{a}+\frac{(A_iB_iC)'}{2A_iB_iC}\dot{a}^2+\frac{(A_iC)'}{2A_iB_iC}\right]\right\}. \tag{2.17b}$$

Remark that, according to the first junction condition and the related discussions, we must have $C_\pm|_a = C$ (Eq. (2.4b)). This is why writing a subindex for C is avoided in the last set of equations. Moreover, according to the positivity of the metric functions, σ is negative-definite so the matter on the throat does not satisfy the weak energy condition and is regarded as exotic. At this point, one could investigate the energy conservation of the throat. The energy conservation for such a structure is given by $\nabla_j S^{ij} = 0$ when $i = \tau$ [29, 98]. The detail of the calculation will not be brought here, however, one must notice that $S^{ij} = h^{jk}S^i_k$, where $h^{jk} = diag(-1, C^{-1}, C^{-1}\sin^{-2}\theta)$, and $\nabla_j S^{ij} = \partial S^{ij}/\partial\zeta_j + \Gamma^i_{jk}S^{kj} + \Gamma^j_{jk}S^{ik}$, where the Christoffel symbols are the ones compatible with the induced metric of the throat h_{ij}. Considering all these, the conservation of energy for the throat turns into

$$C\sigma' + C'(\sigma + p) + \frac{\sigma}{2C'}\left(C'^2 - 2CC''\right) = \frac{C'}{2}\sum_{i=+,-}\left[\frac{(A_iB_i)'}{A_iB_i}\sqrt{\frac{1+B_i\dot{a}^2}{B_i}}\right]. \tag{2.18}$$

In the case $C = r_i^2$, which covers a large class of spherical solutions, the last term on the left-hand side vanishes. Also, the condition $B_i = A_i^{-1}$, which again includes a wide range of solutions, nullifies the term on the right-hand side. For the rest of this study, without loss of generality, we always consider cases in which $B_i = A_i^{-1}$, unless otherwise is stated. However, note that this is not really a restriction, since in general relativity, with proper coordinate transformations, the line elements can always

be written in a fashion where $B_i = A_i^{-1}$. Incidentally, for the solutions which satisfy both conditions, such as the Schwarzschild, the Reissner-Nordström (RN), and the (Anti) de-Sitter solutions ((A)dS), the energy conservation will have the simple form

$$\sigma' + \frac{2}{a}(\sigma + p) = 0. \tag{2.19}$$

As it will be shown in the following sections, the conservation of energy plays a vital role in the mechanical stability of the ATSW. Moreover, it can be perceived from Eq.(2.18) that the tangential pressure p and the energy density σ are not independent quantities and can be considered related through an "Equation of State" or concisely an EoS. Of all the EoSs which have been appeared in the literature, one may enumerates the barotropic EoS [10], the EoS of a (generalized) Chaplygin gas [99], polytropic gas EoS [56], phantom-like EoS [100, 101] and the variable EoS [22]. In this dissertation, we mostly focus on two: the barotropic EoS, given by $p = p(\sigma)$, and a rather generalized form of it, the variable EoS, given by $p = p(\sigma, a)$. In both cases, p represents a differentiable function of its argument(s). Note that, the latter is more appropriate for the TSW perturbations since it involves more degrees of freedom to be accommodated in comparison with the former. In what follows we will use a method called "linear stability analysis" to study the mechanical stability of ATSWs.

2.1.1 Linear Stability Analysis

In this analysis method, developed by Poison and Visser in 1995 [10], firstly, it is assumed that there exists an equilibrium radius a_0, at which the ATSW is stable. Secondly, the throat is being radially perturbed to see whether 1) the throat goes back and settles in a_0 undergoing a (critical) damped oscillations, 2) oscillates about the equilibrium radius a_0 without damping, 3) diverges to infinity, or 4) collapses to zero. Only

in the first case it can be stated that the ATSW is mechanically stable.

Having considered the condition $B_{\pm} = A_{\pm}^{-1}$, we set up the ground by recasting Eq. (2.17a) into the form

$$\dot{a}^2 + V(a) = 0, \tag{2.20}$$

which resembles the equation of conservation of mechanical energy with a kinetic term $\dot{a}^2$ and an effective potential term

$$V(a) = \frac{1}{2}(A_+ + A_-) - \left[\frac{C'(A_+ - A_-)}{2C\sigma}\right]^2 - \left(\frac{C\sigma}{2C'}\right)^2, \tag{2.21}$$

in which $A_{\pm}$, C and σ are all functions of a. In case of a symmetric TSW, for which the connected spacetimes have the same geometrical structure, we have $A_+ = A_- = A$. Hence, the second term identically vanishes whereas the first term simplifies to A. When the ATSW is lying static at its equilibrium radius a_0, it possesses no speed and we have $V_0 \equiv V(a_0) = 0$, according to Eq. (2.20). Once the ATSW is radially perturbed, the effective potential $V(a)$ can be Taylor-expanded about V_0, where for small perturbations we truncate the series by keeping only the first three terms as follows

$$V(a) = V_0 + V_0'(a - a_0) + \frac{1}{2}V_0''(a - a_0)^2 + O^3(a - a_0), \tag{2.22}$$

where $V_0' \equiv \frac{dV(a)}{da}|_{a=a_0}$ and $V_0'' \equiv \frac{d^2V(a)}{da^2}|_{a=a_0}$. The first term on the right-hand side is zero, as discussed above. The second term is also zero, due to the presumption that a_0 is the equilibrium radius, where the tangent to the curve of the potential-radius diagram must vanish. In this regard, the sign of the effective potential, which is now approximated by $V(a) \simeq \frac{1}{2}V_0''(a - a_0)^2$, depends only on the sign of V_0''. Consequently, the ATSW is stable at equilibrium radius a_0, if V_0'' is positive (and so the concavity of the

curve in the potential-radius diagram is upwards), and is unstable at a_0 if V_0'' is negative. In case $V_0'' = 0$, the throat is in a neutral stability which means that when it is slightly perturbed it neither tends to return to its original position nor departs more widely from it. Correspondingly, the next mission will be to compute the explicit form of V_0''. To this end, we start with $V(a)$ in Eq. (2.21) and take the first derivative with respect to a. In the resulted expression, σ' will appear, which should be substituted from Eq. (2.18). Afterwards, the second derivative will be operated, but this time, in addition to σ', we will have $p' \equiv dp(a)/da$ appearing, as well. This is where the EoS enters the calculations. Since the variable EoS $p = p(\sigma, a)$ is a generalization of the barotropic EoS $p = p(\sigma)$, we proceed with the choice of a variable EoS. Whenever needed, just by dismissing the explicit radius-dependency of the pressure, the barotropic EoS might be recovered. Hereupon, for the variable EoS we shall have

$$p' = \omega_1 \sigma' + \omega_2, \tag{2.23}$$

where $\omega_1 \equiv \partial p(\sigma, a)/\partial\sigma$ and $\omega_2 \equiv \partial p(\sigma, a)/\partial a$. Let us note that, after fluid mechanics, ω_1 can naively be taken as the square of the speed of sound in the perfect fluid on the throat. However, for an exotic matter, it does not refer to "the square of the speed of sound" in the usual sense, and indeed, its physical interpretation requires a microphysical model for the throat. To be more specific, constraints such as $\omega_1 > 0$ due to the stable state of the matter, and $\omega_1 \leq 1$ because of the fact that the speed of sound is upper-bounded by the speed of light, do not necessarily apply here. For a detailed discussion see [10]. Nonetheless, we intend to assume that at least the condition $\omega_1 > 0$ is rather realistic, and at some points, discuss the features of stability diagrams on this basis.

After some mathematical calculations and simplifications, the explicit form of V_0'' can be expressed as

$$V_0'' = \frac{1}{4C_0^4 C_0'^2 \sigma_0^4}\Big\{-C_0 C_0'^4 \sigma_0^2 \Big[\left(A_0|_-^+\right)^2 C_0\Big]'' - \left(A_0|_-^+\right)^2 \left(5\sigma_0 p_0 + 6p_0^2\right) C_0'^6$$
$$-8\left(A_0|_-^+\right)\left(A_0'|_-^+\right) C_0 C_0'^5 \sigma_0 p_0 + C_0^4 C_0'^2 \sigma_0^4 \left[-2\sigma_0^2 - 3\sigma_0 p_0 - 2p_0^2 + 2\left(A_{0+}'' + A_{0-}''\right)\right]$$
$$+\sigma_0\Big[\left(A_0|_-^+\right)^2 C_0'^4 - C_0^4 \sigma_0^4\Big]\left[\left(\left(3\sigma_0 + 2p_0\right) C_0'^2 - 2C_0 C_0'' \sigma_0\right)\omega_{10} - 2C_0 C_0' \omega_{20}\right]\Big\} \quad (2.24)$$

where all the functions are calculated at a_0. We have also considered the static versions of the energy density and the tangential pressure, σ_0 and p_0, by setting $a = a_0$ and $\dot{a} = \ddot{a} = 0$ in Eqs. (2.17a, 2.17b) to obtain

$$\sigma_0 = -\frac{C_0'}{C_0}\left(\sqrt{A_{0+}} + \sqrt{A_{0-}}\right) \quad (2.25a)$$

and

$$p_0 = \sqrt{A_{0+}}\left[\frac{A_{0+}'}{A_{0+}} + \frac{C_0'}{C_0}\right] + \sqrt{A_{0-}}\left[\frac{A_{0-}'}{A_{0-}} + \frac{C_0'}{C_0}\right]. \quad (2.25b)$$

Also, the short notation $A_0|_-^+ \equiv A_{0+} - A_{0-}$ has been used. It is obvious that in case of a symmetric TSW where $A_{0+} = A_{0-} = A_0$, the expression for V_0'' widely simplifies to

$$V_0'' = \frac{\left(2A_0 A_0'' - A_0'^2\right) C_0^2 + \left(2A_0 C_0'' + A_0' C_0'\right) A_0 C_0 - 2A_0^2 C_0'^2}{2A_0 C_0^2}$$
$$+ \frac{\left(2A_0 C_0 C_0'' - 2A_0 C_0'^2 + A_0' C_0 C_0'\right)\omega_1}{C_0^2} - \sqrt{A_0}\omega_2. \quad (2.26)$$

Furthermore, if we have $C = a^2$, then

$$V_0'' = \frac{2A_0 A_0'' a_0^2 - A_0'^2 a_0^2 + 2A_0 A_0' a_0 - 4A_0^2}{2A_0 a_0^2} + \frac{2\left(A_0' a_0 - 2A_0\right)\omega_1}{a_0^2} - \sqrt{A_0}\omega_2. \quad (2.27)$$

Having V_0'' calculated, the next mission is to recognize the conditions under which V_0'' is positive. The procedure is simple yet challenging due to some subtleties arising in

some cases. The steps are as follows: We set V_0'' in Eq. (2.24) to zero to write it for ω_{10}. Then, ω_{10} will be graphed against the equilibrium radius a_0, or a redefinition of it. This redefinition is sometimes necessary due to the existence of some other parameters such as mass or charge, which appear in the calculations through the metric functions. On the aforesaid graph, finally, we identify the regions in which V_0'' is positive in value. In these regions, the parameters are such that the ATSW is mechanically stable. In the following section we investigate the mechanical stability of some ATSWs, applying the analysis method above.

2.1.2 Stability of a Cloud-of-Strings ATSW

Let us begin by the simplest example. The geometry of a cloud-of-strings (CoS) is defined by a dust cloud model in which the building blocks of the cloud are classical relativistic strings instead of point particles [102]. The dynamics of such a cloud model is given by a Nambu-Goto action

$$I_{CoS} = \int d\lambda^0 d\lambda^1 M\sqrt{-\gamma}, \tag{2.28}$$

where λ^A are the local coordinates parameterizing the worldsheet of the string, M is a dimensionless non-negative constant characterizing the string by its tension, while $\gamma \equiv \det(\gamma_{AB})$ defines the determinant of the metric tensor $\gamma_{AB} = g_{\alpha\beta}\frac{\partial x^\alpha}{\partial\lambda^A}\frac{\partial x^\beta}{\partial\lambda^B}$ of the string's worldsheet. Here, $g_{\alpha\beta}$ and x^α are the metric tensor and coordinates of the $3+1$-dimensional background spacetime, which for the purpose of this section is considered to be flat. The solution, therefore, is given by [102, 103]

$$ds^2 = kdt^2 + k^{-1}dr^2 + r^2 d\Omega^2 \tag{2.29}$$

where $k > 1$ is a constant related to the proper density of the string cloud. Comparing Eq. (2.29) to Eq. (2.1) one gets

$$\begin{cases} A_{\pm} = k_{\pm} \\ C_{\pm} = r_{\pm}^2 \end{cases} \tag{2.30}$$

for the metric functions of the side-spacetimes. Before we proceed, and in order to provide ourselves with mathematical means which clearly reflect the asymmetry of the side-spacetimes, let us redefine $k_{\pm}$ with $k_{-} \equiv k$ and $k_{+} \equiv (1+\epsilon)\,k$, and call ϵ the asymmetry factor of the ATSW. Since $k_{-} > 1$ and $k_{+} > 1$, the admissible domain of ϵ is $[0,\infty)$, with $\epsilon = 0$ referring to a usual symmetrical TSW. Considering the metric functions, the effective potential V_0'' in Eq. (2.24) simplifies to

$$V_0'' = -2\sqrt{1+\epsilon}\left(\frac{2\omega_{10}+1}{x_0^2} + \frac{\tilde{\omega}_{20}}{1+\sqrt{1+\epsilon}}\right), \tag{2.31}$$

where we have introduced the reduced equilibrium radius $x_0 \equiv a_0/\sqrt{k}$ and applied the redefinition $\tilde{\omega}_{20} \equiv \sqrt{k}\omega_{20}$, in order to excise k out of the calculations. Setting V_0'' to zero in Eq. (2.31), one recovers "the square of the speed of sound" as

$$\omega_{10} = -\frac{1}{2}\left(1 + \frac{\tilde{\omega}_{20}x_0^2}{1+\sqrt{1+\epsilon}}\right). \tag{2.32}$$

It can easily be seen, that in case of a barotropic EoS ($\tilde{\omega}_{20} = 0$) we have $\omega_{10} = -1/2$, regardless of the values of the asymmetry factor ϵ, the metric parameter k, or even the equilibrium radius a_0. However, for any physically meaningful (to the best of our knowledge) values of $\omega_{10} \in (0,1)$, the potential is negative, back to Eq. (2.31). This implies that a TSW, either symmetric or asymmetric, cannot be supported by a barotropic fluid on its throat. On the other hand, a reasonable variable EoS ($\tilde{\omega}_{20} \neq 0$), with sufficiently negative $\tilde{\omega}_{20}$ will lead to a meaningful ω_{10}, and hopefully a positive V_0''. For example, let us simply consider $\tilde{\omega}_{20} = -6/x_0^2$. Therefore, for any $\epsilon \in [0,24)$, ω_{10} in Eq. (2.32) is in the range $(0,1)$. However, note that $\tilde{\omega}_{20}$ being negative does

not imply a negative pressure, since $\tilde{\omega}_{20} \propto \frac{\partial p}{\partial a}|_{a_0}$ only represents a gradient in pressure, by definition. Fig. 2.1 has been plotted for ω_{10} against x_0 for different values of ϵ when $\tilde{\omega}_{20} = -6/x_0^2$. The regions marked with an "S" are where the effective potential is positive, hence, the ATSW is mechanically stable. The important remark here is that as the side-universes become more and more asymmetric with an increase in the asymmetry factor ϵ, the stability region shrinks and as an outcome, the number of the pairs (a_0, ω_{10}) which result in a positive effective potential decreases. This, somehow, can be interpreted as the following: the odds to have a stable ATSW decreases by an increase in the asymmetry factor ϵ; or, in other words, a symmetric TSW has a better chance to be stable than an asymmetric one. Note that, setting $k = 1$ and $\epsilon \neq 0$ leads to a CoS-Minkowski ATSW, while the case $k = 1$ and $\epsilon = 0$ is just a usual Minkowski TSW. One can easily confirm that the discussions in the lines above applies to both of these special cases, as well.

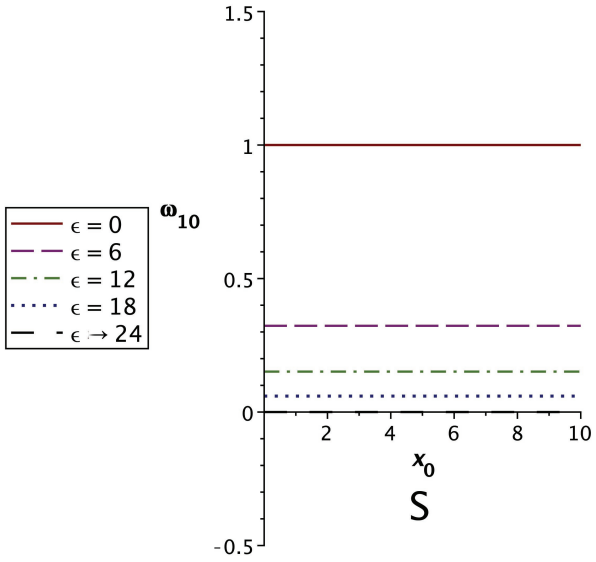

Figure 2.1: The graph shows ω_{10} against x_0 for different values of ϵ when $\tilde{\omega}_{20} = -6/x_0^2$. The regions underneath the lines are where the ATSW is mechanically stable.

It was observed that, in general, a CoS ATSW cannot be supported by a barotropic fluid. This obstacle, however, can be lifted by exploiting a variable EoS type of fluid at the throat, instead of a barotropic fluid. As it was explained, in variable EoS, unlike in barotropic EoS, there exists an explicit radial-dependency for the pressure of the fluid at the throat, which is represented by $\tilde{\omega}_{20}$. To see the impact of $\tilde{\omega}_{20}$ more visibly, let us solve $V_0'' = 0$ in Eq. (2.31) for $\tilde{\omega}_{20}$ instead of ω_{10}. The result is

$$\tilde{\omega}_{20} = -\frac{(2\omega_{10}+1)\left(1+\sqrt{1+\epsilon}\right)}{x_0^2}. \tag{2.33}$$

From the form of this function, it is easy to see that for a constant ω_{10} and a constant ϵ, the magnitude of $\tilde{\omega}_{20}$ decreases inversely by x_0^2. This admits that the greater the equilibrium radius is, the less the effective is the variable EoS's impact (Compared with the barotropic EoS). What is more, for a constant ω_{10} in constant reduced equilibrium radius x_0, the magnitude of $\tilde{\omega}_{20}$ grows larger by ϵ. This means that the more asymmetric the ATSW becomes, the role of the variable EoS becomes more outstanding, although the rate of its growth decreases due to the square root. Fig. 2.2 summarizes the results.

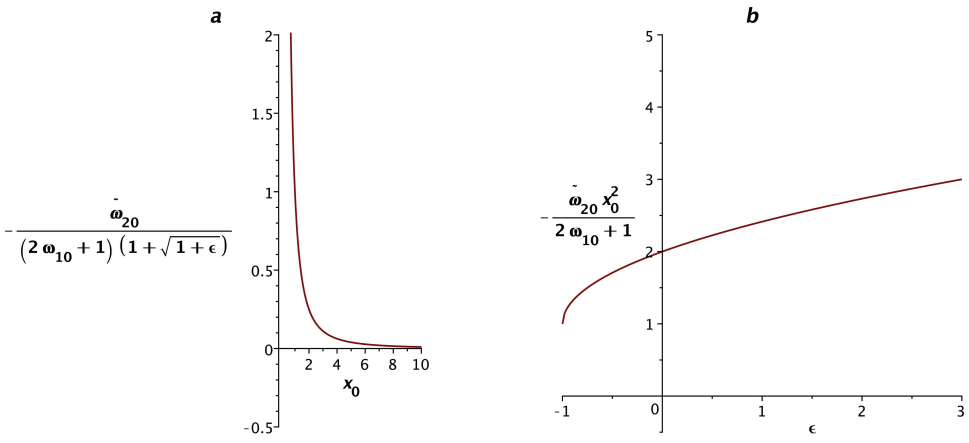

Figure 2.2: The diagrams show a) $\tilde{\omega}_{20}$ versus x_0 for constant ω_{10} and ϵ, and b) $\tilde{\omega}_{20}$ versus ϵ for constant ω_{10} and x_0, for a CoS ATSW with a variable EoS.

2.1.3 Stability of a Schwarzschild ATSW

In this section and the nexts, the EoS under consideration will be the barotropic EoS. We will come back to the variable EoS in section 2.2, where we address the discontinuity problem in the stability diagrams. As the next example, we look at the case in which the throat provides a transition between two Schwarzschild geometries possessing different central masses. In other words, we require

$$\begin{cases} A_{\pm} = 1 - \frac{2m_{\pm}}{r_{\pm}} \\ C_{\pm} = r_{\pm}^2 \end{cases} \tag{2.34}$$

for the two side spacetimes, where analogous to the previous section, we define an asymmetry factor $\epsilon \in [-1, \infty)$, such that $m_- \equiv m$ and $m_+ \equiv (1+\epsilon)\, m$. Each spacetime has an event horizon at $r_{eh\pm} = 2m_{\pm}$, so the equilibrium radius a_0 must always be greater than the greatest of these event horizon radii. From Eq. (2.24), $V''(a_0)$ can be solved to obtain ω_{10} in terms of ϵ, ω_{20} and x_0, where $x_0 \equiv a_0/m$ is the reduced radius. Here, to avoid the awkwardness due to their very long mathematical forms, we refrain from bringing $V''(a_0)$ and ω_{20} explicitly. Instead, by analyzing the associated graphs we will point out the important remarks. In the case of a barotropic EoS ($\omega_{20} = 0$), one can plot ω_{10} against x_0 for various values of ϵ. It is not hard to see that for the special case of $\epsilon = 0$, the symmetric Schwarzschild TSW studied by Poisson and Visser in [10] revives; the throat connects two Schwarzschild geometries with the same central masses. Also, it is worth mentioning that for $\epsilon = -1$ the wormhole couples a Schwarzschild spacetime with a flat Minkowski spacetime. In Fig. 2.3 the graphs for ω_{10} against x_0 are depicted for six different values of ϵ. Regions with an S are the regions of stability for the wormhole where $V''(a_0)$ is evidently positive. According to Fig. 2.3, as ϵ increases from -1 to 0 (as the mass m_+ grows from 0 to m), the reduced event horizon $x_{eh} \equiv$

r_{eh}/m, which belongs to the greater mass $m_- = m$, remains unchanged. Once the value of ϵ passes zero upwards, the reduced horizon is divided by $m_+ = (1+\epsilon)m$. For all the values of ϵ considered here, the graphs keep exhibiting a similar character to the symmetric case at $\epsilon = 0$, consisting of a bowl-like branch followed first by a discontinuity, and then by an asymptotically growing-to-zero branch. The square of the speed of sound ω_{10} is always positive for the stability region of the bowl-like branch in Fig. 2.3. The figure indicates that any deviation from symmetric case with $\epsilon = 0$, makes the region of stability smaller. This is the evidence that, at least for the physically meaningful values of ω_{10}, the more symmetric the TSW is, the more likely it is to find it in a stable state against a radial perturbation. The discontinuity in the stability diagram lies in the very heart of the definition of ω_{10}. In section 2.2 we will surgically revisit this issue. There, we will show how substituting the barotropic EoS with a well-tuned variable EoS helps to remove this discontinuity.

2.1.4 Stability of an Extremal Reissner-Nordström ATSW

As the next example, let us investigate the behavior of an ATSW which connects two extremal Reissner-Nordström (ERN) spacetimes. After the Schwarzschild solution, the RN geometry is the second famous black hole solution of the Einstein's field equations. It actually generalizes the massive and non-rotating Schwarzschild black hole to a massive, non-rotating and charged black hole with the mass m and the charge q. (In fact q^2 is the sum of the squares of the net electric and magnetic charges of the black hole). The line element of RN spacetime is given as

$$ds^2 = -\left(1 - \frac{2m}{r} - \frac{q^2}{r^2}\right) dt^2 + \left(1 - \frac{2m}{r} - \frac{q^2}{r^2}\right)^{-1} dr^2 + r^2 d\Omega^2, \tag{2.35}$$

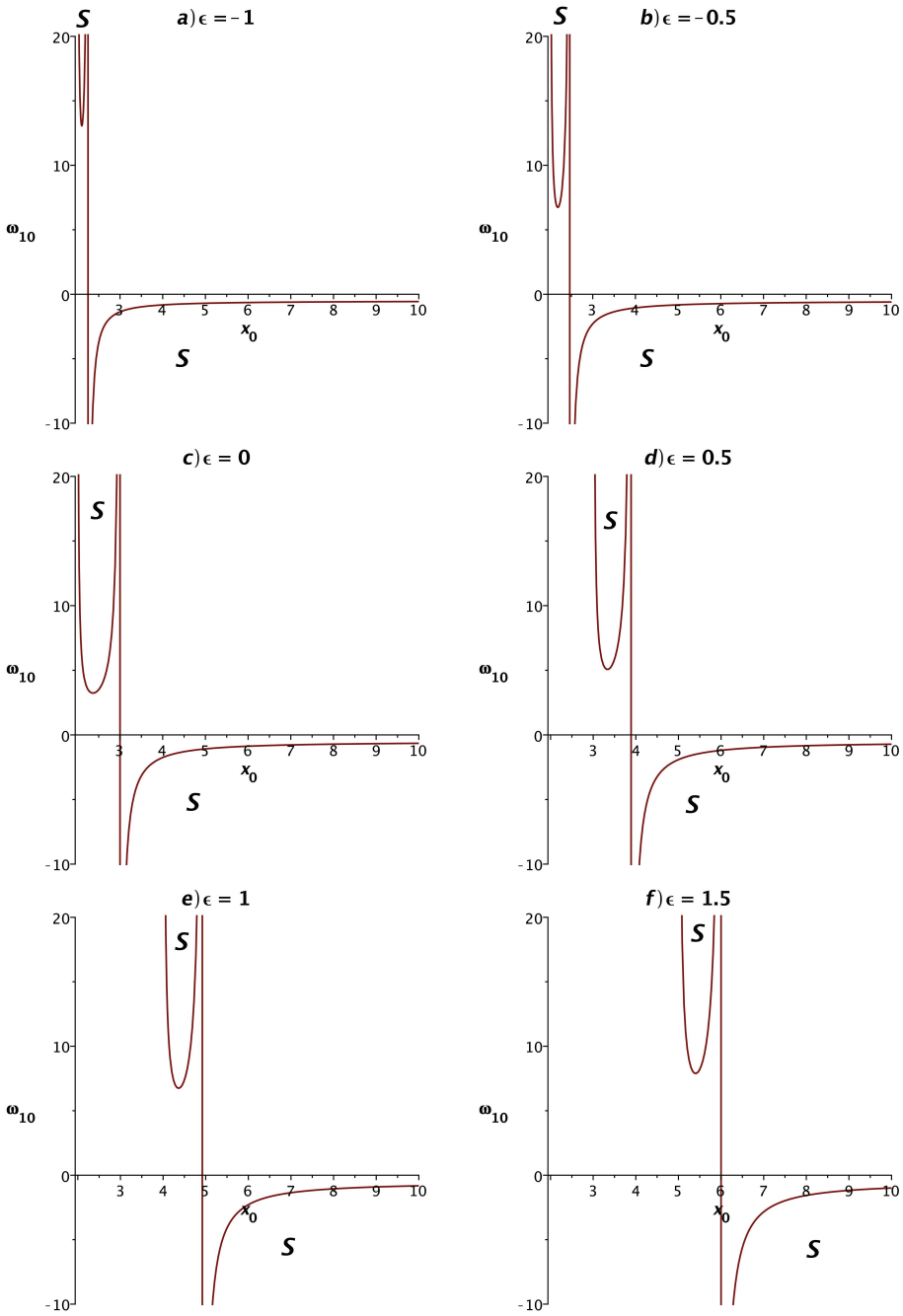

Figure 2.3: The plots of ω_{10} versus x_0 with different values of ϵ for a Schwarzschild ATSW with barotropic EoS. The stable regions are marked with an "S".

with an event and an inner horizon at $r_{eh} = m + \sqrt{m^2 - q^2}$ and $r_{ih} = m - \sqrt{m^2 - q^2}$, respectively. (Note that with respect to the unit convention used here, mass and charge have the same dimensionality). If $|q| \leq m$, then r_h is real and the singularity is hidden behind the event horizon, while for $|q| > m$ the spacetime exhibits a naked singularity. The special case of $|q| = m$ occurs when the two horizons coincide and an ERN spacetime eventuates. Consequently, the line element of ERN can be written as

$$ds^2 = -\left(1 - \frac{m}{r}\right)^2 dt^2 + \left(1 - \frac{m}{r}\right)^{-2} dr^2 + r^2 d\Omega^2, \tag{2.36}$$

with an event horizon at $r_{eh} = m$. The case of a usual symmetric ERN TSW has been studied in the literature [25,28,64]. However, for the purpose of constructing an ATSW, let us have

$$\begin{cases} A_\pm = \left(1 - \frac{m_\pm}{r_\pm}\right)^2 \\ C_\pm = r_\pm^2 \end{cases}. \tag{2.37}$$

where analogous to the previous section we have $m_- \equiv m$ and $m_+ \equiv (1+\epsilon)\, m$, where $\epsilon \in [-1, \infty)$ is the asymmetric factor. The steps leading to ω_{10} is also similar to the previous section. With these settings, the respective ω_{10} for an ERN ATSW is plotted against $x_0 \equiv a_0/m$ in Fig. 2.4, for a barotropic fluid on the throat ($\omega_{20} = 0$) and different values of ϵ. The stable regions are also shown. Although the location of the event horizon and the discontinuity are different from the Schwarzschild ATSW, the results are very similar. Firstly, the general shapes of the graphs and the stability regions are the same. Secondly, the most likely stable configuration is the one of the symmetric case, where $\epsilon = 0$, in the sense that more (x_0, ω_{10})-pairs are available in this configuration such that $V''(a_0) > 0$.

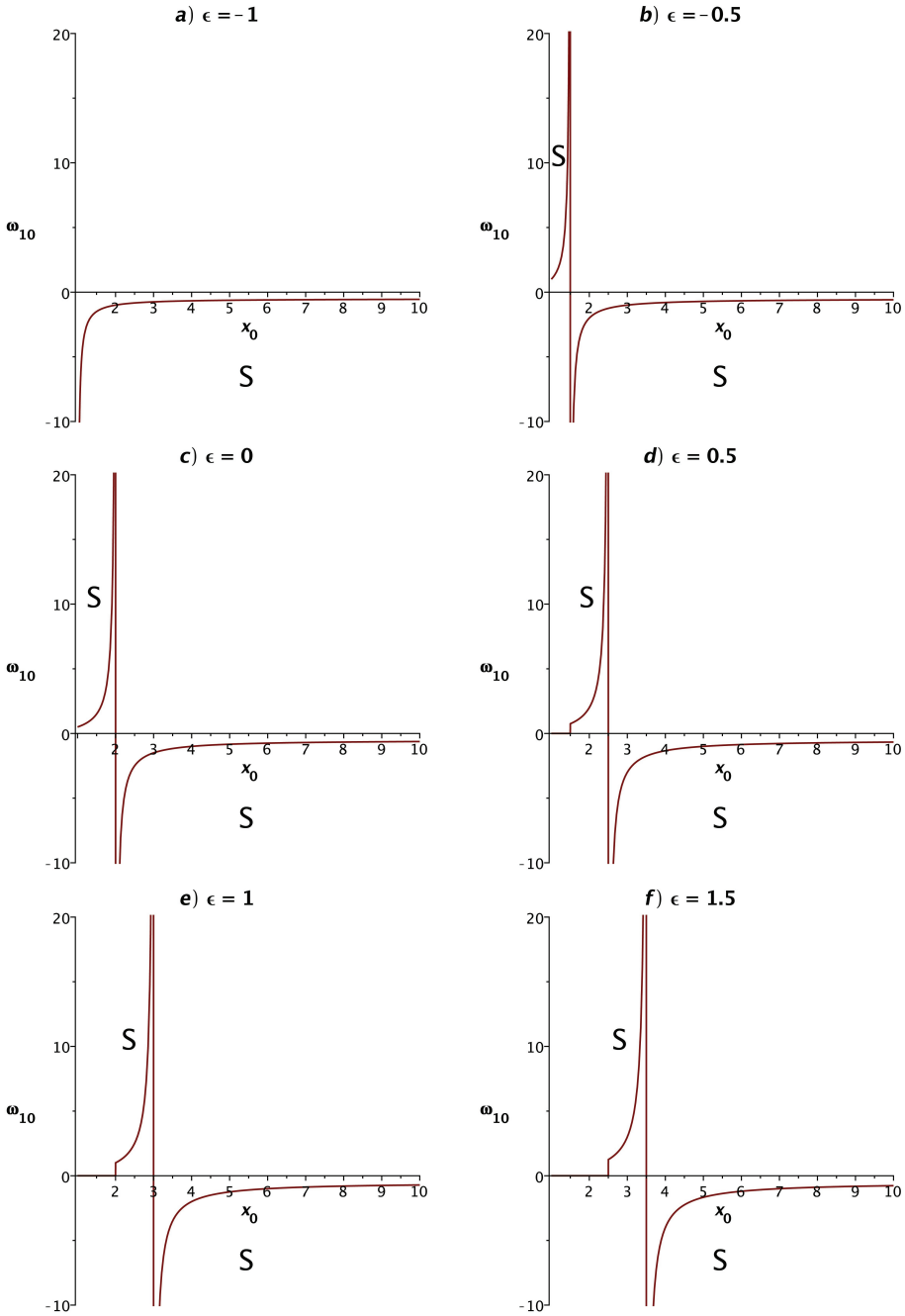

Figure 2.4: The plots of ω_{10} versus x_0 with different values of ϵ for a ERN ATSW with barotropic EoS. The stable regions are marked with an "S".

2.1.5 Stability of a Schwarzschild-Reissner-Nordström ATSW

As the next example, let us investigate the behavior of an ATSW which connects two inherently different spacetimes; a Schwarzschild geometry with a central mass $m_- \equiv m$ and an RN geometry with a central mass $m_+ \equiv (1+\epsilon)\,m$ and a non-zero total charge q. Hereupon, we demand

$$\begin{cases} A_- = 1 - \frac{2m_-}{r_-} \\ A_+ = 1 - \frac{2m_+}{r_+} + \frac{q^2}{r_+^2} \\ C_\pm = r_\pm^2 \end{cases}, \tag{2.38}$$

for the two side-spacetimes. Due to our unit convention, we are allowed to express q in terms of m in the fashion $q = \zeta m_+$, where ζ is a real number. Inserting all these into Eq. (2.24) beside considering a barotropic EoS, results in an expression for $V''(a_0)$ in terms of a_0, ϵ, ζ, ω_{10} and m. Equating $V''(a_0)$ to zero, one can untangle ω_{10} in terms of the remaining parameters. Needless to say, interpolating the parameters included can produce a huge number of combinations, each having the potential to be the subject for a separate detailed study in the future. However, here in this account, we wrap it up with a single example of a very specific case in which $\epsilon = 0$ and $\zeta = 1$; accordingly, $m_- = m_+ = q = m$. Evidently, this grants the special case of ERN geometry for one of the spacetimes. Hence, the expression for ω_{10} reduces to

$$\omega_{10} = -\frac{3\sqrt{x_0}\,(x_0-2)^{3/2} + x_0}{2\,(x_0-2)\,(3x_0-8)} \tag{2.39}$$

where in analogy with the previous sections, $x_0 \equiv a_0/m$. As shown in Fig. 2.5, the stability diagram for ω_{10} surprisingly depicts the same general configuration as the ones in the previous sections. Note that the event horizon of the Schwarzschild spacetime is at $2m$ while the event horizon of the ERN spacetime is at m. Therefore, we must have

$a_0 > 2m$ or $x_0 > 2$. Based on this, unlike what one naively concludes from Eq. (2.39), there is only one discontinuity in the stability diagram at $x_0 = 8/3$. Furthermore, the subtle reader would note that if we had set $\zeta = 0$, the discussions represented in section 2.1.2 for the Schwarzschild ATSW would be recovered.

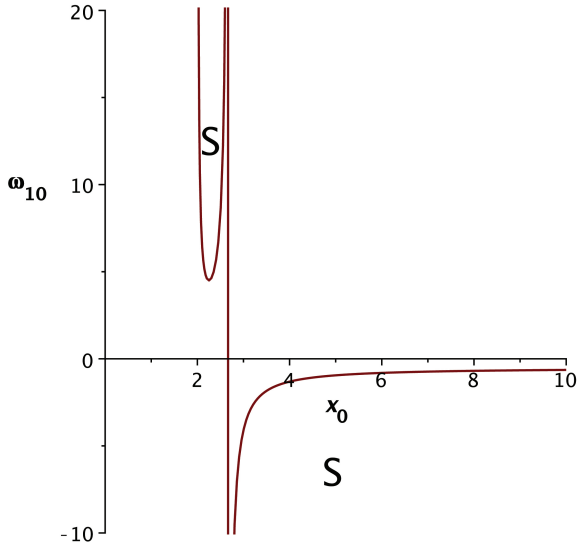

Figure 2.5: The plots of ω_{10} versus x_0 with for a Schwarzschild-ERN ATSW with $\epsilon = 0$, $\zeta = 1$ and barotropic EoS. The stable regions are marked with an "S".

2.1.6 Stability of a de-Sitter-Anti de-Sitter ATSW

As the last example, let us study an interesting case in which a de Sitter (dS) universe meets an anti-de Sitter (AdS) universe with the same cosmological constant at the throat of an ATSW. (A)dS geometries are the simplest solutions to the Einstein's field equations with a non-vanishing cosmological constant Λ. Usual symmetric TSWs in Schwarzschild-de-Sitter and Schwarzschild-Anti de-Sitter spacetimes has been studied before [104, 105]. Here we consider the metric functions as

$$\begin{cases} A_\pm = 1 \pm \frac{r_\pm^2}{\alpha^2} \\ C_\pm = r_\pm^2 \end{cases}, \tag{2.40}$$

where the $+$ $(-)$ sign represents AdS (dS) geometry. Also, we have $\alpha^2 = 3/\Lambda$ for dS and AdS, respectively, where Λ is the cosmological constant (positive for dS and negative for AdS). Note that for the dS universe there is a cosmological horizon at $r_{ch} = \alpha$. Joining these two universes by cut-and-paste procedure at their common timelike hypersurface at $a_0 < \alpha$, gives rise to a dS-AdS ATSW, for which

$$\omega_{10} = -\frac{2 - \sqrt{1 - x_0^4}}{2\left(1 - x_0^4\right)}. \tag{2.41}$$

Herein, we have defined $x_0 \equiv a_0/\alpha$, where $x_0 < 1$. The associated stability diagram along with the mechanically stable region is given in Fig. 2.6. As it can be seen, there is no discontinuity corresponding to this ATSW. However, the dS-AdS ATSW is stable only for negative values of ω_{10}, which is not meaningful, from a physical point of view.

Here we investigated some examples for ATSWs. However, there are many more choices to be studied within this framework. For instance, any other combinations of the Schwarzschild, the Reissner-Nordström and the (Anti) de-Sitter spacetimes that we have not considered here, could potentially be a test bed for ATSWs.

2.2 Infinite Discontinuity in the Stability Diagram

In this section, we address to a particular issue of stability which incorporates infinite discontinuity in the stability diagrams of some ATSWs we have investigated in the previous section. The divergence radius occurs at a finite radius which lies outside the event horizon and inside the cosmological horizon (if any), excluding the divergences at the center and at infinity. What gives rise to this behavior? Is it possible to eliminate these types of divergences? When a barotropic EoS is in operation, we observed that such discontinuities occurred in the stability diagrams of the Schwarzschild ATSWs,

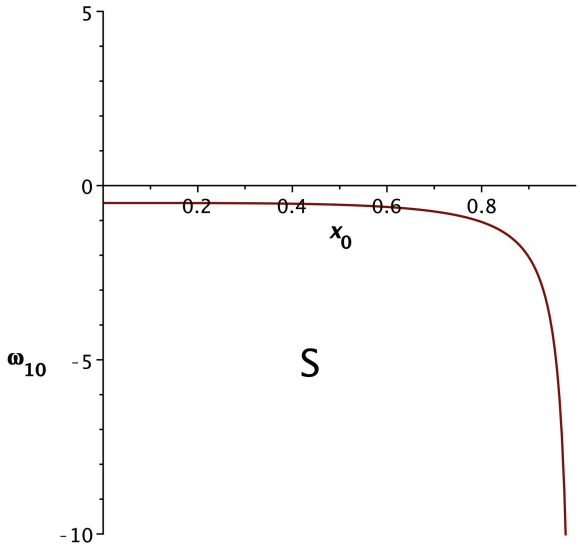

Figure 2.6: The plots of ω_{10} versus x_0 with different values of ϵ for a Schwarzschild ATSW with barotropic EoS. The stable regions are marked with an "S".

the ERN ATSWs, and the Schwarzschild-ERN ATSWs, due to amplitude-divergences in ω_{10}. However, they did not emerge in the corresponding stability diagrams of the CoS ATSWs and the dS-AdS ATSW. Firstly, we will explain this by spotting the origin of such discontinuities, and then, as they are physically non-acceptable, we eliminate them systematically by revising the EoS and fine-tuning the pressure at equilibrium.

Previously, we have observed that for the barotropic EoS we have $p_0' = \omega_{10}\sigma_0'$ at the throat. Exercising this on the static version of Eq. (2.18) leads to

$$\omega_{10} = \frac{p_0'}{-\frac{C_0'}{C_0}(\sigma_0 + p_0) + \frac{2C_0C_0'' - C_0'^2}{2C_0C_0'}\sigma_0}, \tag{2.42}$$

which goes to infinity once the denominator goes to zero, unless $p_0' \to 0$ faster. Therefore, the infinite discontinuity is fundamental and cannot be removed by, say, changing the coordinates. In a case where $C(a) = a^2$, the above equation reduces to the simpler

form

$$\omega_{10} = \frac{p_0'}{-\frac{2}{a_0}(\sigma_0 + p_0)}. \tag{2.43}$$

In such a case, $\sigma_0 + p_0 \to 0$ faster than $p_0' \to 0$ leads to an infinite discontinuity. Here we proceed with some examples.

The Schwarzschild ATSW: It is well-known that for a symmetric Schwarzschild TSW there exists an infinite discontinuity at $a_0 = 3m$, where m is the central mass of the Schwarzschild spacetime [10]. More generally, for a Schwarzschild ATSW with metric functions given in Eq. (2.34) we obtain

$$\begin{aligned}\sigma_0 + p_0 = -\frac{1}{a_0^{3/2}\left[a_0 - 2(1+\epsilon)m\right](a_0 - 2m)} \times \\ \left\{\left[a_0 - 3(1+\epsilon)m\right](a_0 - 2m)\sqrt{a_0 - 2(1+\epsilon)m}\right. \\ \left. + \left[a_0 - 2(1+\epsilon)m\right](a_0 - 3m)\sqrt{a_0 - 2m}\right\}.\end{aligned} \tag{2.44}$$

where we have used $m_- \equiv m$ and $m_+ \equiv (1+\epsilon)m$. This has a double root at

$$a_{\mathrm{ID}_\pm} = \frac{3m}{8}\left[3(\epsilon+2) \pm \sqrt{9\epsilon^2 + 4\epsilon + 4}\right], \tag{2.45}$$

where the sub-index "ID" stands for infinite discontinuity. However, for the admissible domain of ϵ, the root with the minus sign falls behind the event horizon, i.e. $a_{\mathrm{ID}_-} < r_{eh}$, whereas $a_{\mathrm{ID}_+} > r_{eh}$ always holds. Hence, an infinite discontinuity is expected at a_{ID_+}, which obviously leads to $a_{\mathrm{ID}} = 3m$ for a symmetric Schwarzschild TSW with $\epsilon = 0$. Fig. 2.7, which illustrates $m(\sigma_0 + p_0)$ versus a_0/m for the symmetric case, explains why $\lim_{a_0 \to 3m^\pm} \omega_{10} = \mp\infty$.

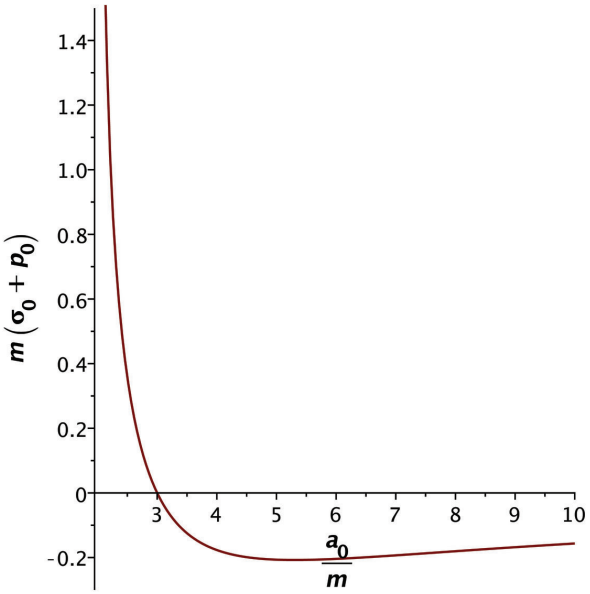

Figure 2.7: The graph shows $m(\sigma_0 + p_0)$ versus a_0/m for a symmetric Schwarzschild TSW. At $a_0 = 3m$, $m(\sigma_0 + p_0) = 0$ which validates the previous results. Note that while $\sigma_0 + p_0$ is positive valued pre-$3m$, it is negative post-$3m$. This explains $\lim_{a_0 \to 3m^{\pm}} \beta_0^2 = \mp\infty$ in the original stability diagram.

The Extremal Reissner-Nordström TSW: The case of an extremal Reissner-Nordström (ERN) TSW has also been considered in the literatures [25, 28, 29]. Given Eq. (2.37), as the metric functions corresponding to the bulk spacetimes of the ERN ATSW, we obtain

$$\sigma_0 + p_0 = -\frac{2\left[a_0 - (\epsilon + 2)\, m\right]}{a_0^2}. \tag{2.46}$$

Accordingly, there must be an infinite discontinuity at

$$a_{\rm ID} = (\epsilon + 2)\, m. \tag{2.47}$$

As shown in [28], this also admits an infinite discontinuity at $a_0 = 2m$ for a symmetric ERN TSW, when $\epsilon = 0$. For such a symmetric TSW, analogous to the previous case, $\lim_{a_0 \to 2m^{\pm}} \omega_{10} = \mp\infty$, according to Fig. 2.8 plotted for $m(\sigma_0 + p_0)$ versus a_0/m.

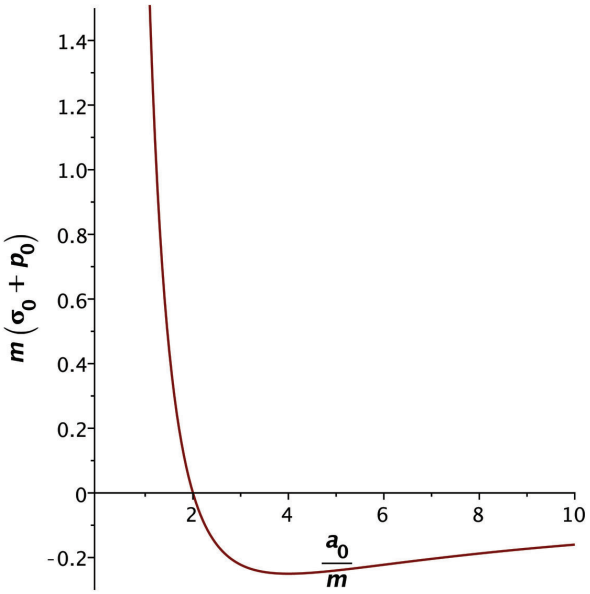

Figure 2.8: The graph of $m(\sigma_0 + p_0)$ against a_0/m for a symmetric ERN TSW. The zero of the vertical axis at $a_0 = 2m$ is expected according to the previous studies.

The Dilaton TSW: In [31, 106], Eiroa studies a TSW constructed by two symmetric spacetimes which are solutions of the action

$$I = \int d^4x\sqrt{-g}\left[-R + (\nabla\phi)^2 + e^{-2b\phi}F^2\right]. \tag{2.48}$$

Herein, $g = \det(g_{\mu\nu})$, R is the Ricci scalar, ϕ is the scalar dilaton field, $F = F^{\mu\nu}F_{\mu\nu}$ with $F_{\mu\nu}$ being the electromagnetic field, and $b \in [0,1]$ is the coupling parameter between the dilaton and the electromagnetic field. In Schwarzschild coordinates, the spherically symmetric solution is given by

$$ds^2 = -A(r)\,dt^2 + A^{-1}(r)\,dr^2 + C(r)\,d\Omega^2 \tag{2.49}$$

where the metric functions are [107, 108]

$$\begin{cases} A(r) = \left(1 - \frac{M}{r}\right)\left(1 - \frac{Q}{r}\right)^{\left(1-b^2\right)/\left(1+b^2\right)} \\ C(r) = r^2\left(1 - \frac{Q}{r}\right)^{2b^2/\left(1+b^2\right)} \end{cases}. \tag{2.50}$$

The constants M and Q are related with the mass m and charge q of the spacetime through

$$\begin{cases} M = m \pm \sqrt{m^2 - (1-b^2)\,q^2} \\ Q = \left(1+b^2\right) q^2/M \end{cases} . \tag{2.51}$$

Here we consider only the plus sign, because it is the plus sign that corresponds to the Schwarzschild metric when $q = 0$. The solutions for $b = 0$ reduce to the normal RN solutions for the Einstein-Maxwell action with a scalar field. For $b = 1$ a family of static, spherically symmetric charged solutions in the context of low-energy string theory are recovered [107]. Moreover, for $0 \leq q^2/m^2 < 1 + b^2$ the solution is a black hole with an event horizon at $r = M$ and an inner horizon at $r = Q$. When $1 + b^2 \leq q^2/m^2 \leq 1/\left(1-b^2\right)$, the inner horizon grows larger than the event horizon and the metric exhibits a naked singularity. Also, the spacetime is not well-defined if $q^2/m^2 > 1/\left(1-b^2\right)$. In what follows a_0 is considered to be greater than M and Q, as it must be.

According to the solution in Eqs. (2.50) and (2.51), it is expected that the root of the denominator in the expression for ω_{10} in Eq. (2.42) denotes the infinite discontinuity in the stability diagram. Having the static energy density as

$$\sigma_0 = -2\frac{C_0'}{C_0}\sqrt{A_0}, \tag{2.52a}$$

and the static pressure as

$$p_0 = \left(\frac{A_0'}{A_0} + \frac{C_0'}{C_0}\right)\sqrt{A_0}, \tag{2.52b}$$

one calculates for the roots of the denominator of ω_{10} in Eq. (2.42), to acquire a_{ID}. Due to the relatively complicated forms of $A(r)$ and $C(r)$ in Eq. (2.50), the expression

for $a_{\rm ID}$ is complicated and lengthy, too. For this reason, we refrain from bringing its explicit form here. Instead, we summarize the results in Fig. 2.9. Considering five different values for b, the subfigures display $a_{\rm ID}$, the event horizon (EH) associated with $r = M$, and the inner horizon (IH) associated with $r = Q$, in diagrams of $a_{\rm ID}/m$ against $|q|/m$. The results are in complete agreement with the ones in [31]. For instance, for $b = 0$ in Fig. 2.9 a, there always exists an infinite discontinuity beyond horizons. In the numerical examples, this discontinuity is $a_{\rm ID_+} = 3m$ for $|q|/m = 0$, and $a_{\rm ID_+} \simeq 2.485m$ for $|q|/m = 0.8$, as expected. Note that $|q|/m > 1$ is not allowed due to the restricting conditions on the bulk spacetime mentioned above. On the other hand, when $b = 1$, there is no infinite discontinuity for $|q|/m \geq \sqrt{2}$. Again, for the sake of comparison to the results in [31], note that, for example, when $|q|/m = 0.8$ we obtain $a_{\rm ID} \simeq 2.594m$, and $a_{\rm ID} \simeq 2.860m$, when $b = 0.5$, and $b = 1$, respectively. Furthermore, remark that $a_{\rm ID}$ is $3m$ in all cases, when $|q|/m = 0$, due to the simple fact that when $q = 0$, the metric functions in Eq. (2.50) reduce to the Schwarzschild metric functions, regardless of the value of b.

2.2.1 Variable EoS

In 2015, Varela demonstrated that the infinite discontinuity of a Schwarzschild TSW can be removed by using the variable EoS [22]. As it was discussed, the variable EoS grants the pressure an explicit radius-dependency. The mechanism of infinite discontinuity removal by the variable EoS is simply to null the numerator of

$$\omega_{10} = \frac{p_0' - \omega_{20}}{-\frac{C_0'}{C_0}(\sigma_0 + p_0) + \frac{2A_0A_0'' - A_0'^2}{2A_0A_0'}\sigma_0} \tag{2.53}$$

at $a_{\rm ID}$, where the discontinuity had happened when ω_{20} was zero. This means, if we

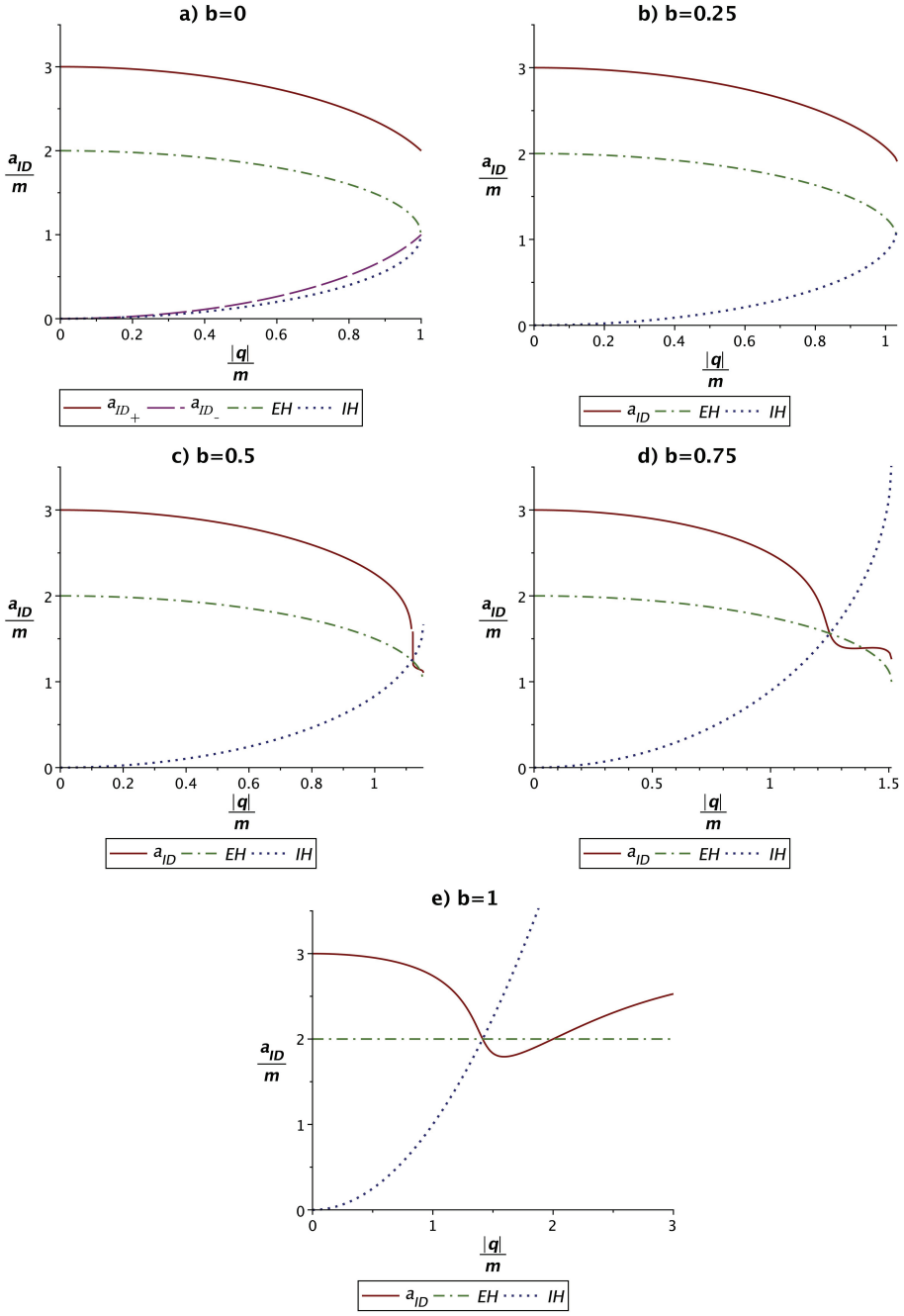

Figure 2.9: The graphs show a_{ID}/m against $|q|/m$ for a dilaton TSW for different values of b. In the legend, a_{ID_+} and a_{ID_-} correspond to the roots of the denominator of β_0^2, given by Eq. (30). Also, EH and IH correspond to the event horizon and the inner horizon of the bulk universe.

set ω_{20} such that

$$\omega_{20} = p_0', \tag{2.54}$$

then $\lim_{a_0 \to a_{\mathrm{ID}}} \omega_{10} = \frac{0}{0}$ is indefinite, and it becomes well-defined if the numerator approaches zero, at least, at the same rate as the denominator. As far as the unit convention that is applied here concerns, ω_{10} is a dimensionless quantity ($\omega_{10}^{1/2}$ is of type speed, with the SI dimension $\left[LT^{-1}\right]$, which becomes dimensionless here, since length and time are looked at on an equal footing in general relativity). Hereupon, the numerator and the denominator of ω_{10} have the same dimension (L^{-2}), and in case the fine-tuning $\omega_{20} = p_0'$ is exerted, ω_{10} can be well-defined. Note that Eq. (2.53) is somehow a generalization to Eq. (2.42).

For the case of a symmetric Schwarzschild TSW one obtains

$$p_0'\big|_{a_0=3m} = -\frac{2\sqrt{3}}{9m^2}, \tag{2.55}$$

by taking the first derivative of Eq. (2.17b) (with $B_i = A_i^{-1}$), applying Eq. (2.34) and setting $\epsilon = 0$. This means that by fine-tuning ω_{20} to $-2\sqrt{3}/\left(9m^2\right)$ we might be free from infinite discontinuity in the stability diagram. This is particularly shown in Fig. 2.10 for ω_{10} against a_0/m. As it is evident, there is no sign of the infinite discontinuity anymore.

Applying the variable EoS to an ERN ATSW leads to the same result. In this case we obtain

$$p_0'\big|_{a_0=(\epsilon+2)m} = -\frac{2}{(\epsilon+2)^2 m^2}, \tag{2.56}$$

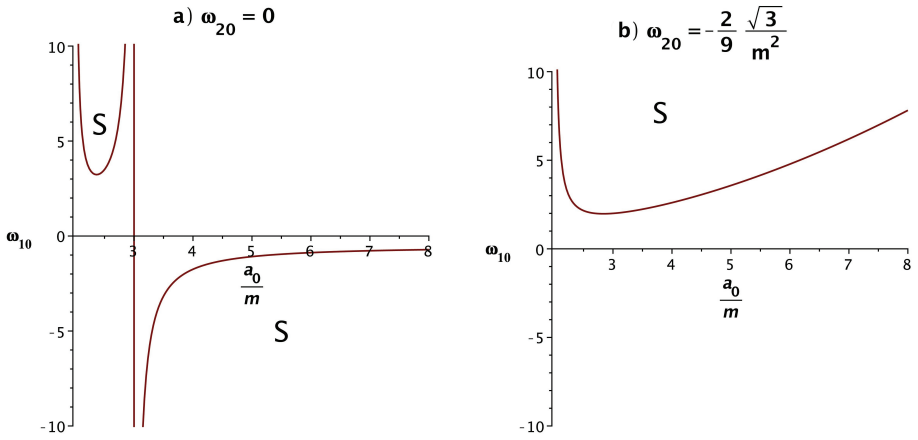

Figure 2.10: The stability diagram for a symmetric Schwarzschild TSW with a) the barotropic EoS and b) the variable EoS. It can be observed that the infinite discontinuity is simply removed by virtue of the variable EoS.

as the derivative of the angular pressure at the radius of infinite discontinuity occurrence. Correspondingly, the choice $\omega_{20} = -2/\left((\epsilon+2)^2 m^2\right)$ is expected to remove the infinite discontinuity. Fig. 2.11 shows how this happens for a symmetric ERN TSW, for which $\epsilon = 0$.

In the end, we turn our attention to the dilaton TSW. Here, we take a closer look at three cases for which $b = 0$, $b = 0.5$, and $b = 1$. The first is selected because it defines the RN spacetime, and the last is selected for its importance in string theory. The choice $b = 0.5$ is rather random, as an intermediate value in the b-spectrum. Also, for all three cases, without loss of generality, we have randomly chosen $|q|/m = 0.5$. Our numerical analyses show that for the three cases we have

$$\begin{cases} p_0'\big|_{a_0=a_{\rm ID}} \simeq -0.4139864432/m^2 & \text{when} \quad b=0 \\ p_0'\big|_{a_0=a_{\rm ID}} \simeq -0.4146553639/m^2 & \text{when} \quad b=0.5 \\ p_0'\big|_{a_0=a_{\rm ID}} \simeq -0.4162095590/m^2 & \text{when} \quad b=1 \end{cases}, \tag{2.57}$$

which denotes that if we fine-tune ω_{20} such that $\omega_{20}|_{b=0} = -0.4139864432/m^2$, $\omega_{20}|_{b=0.5} =$

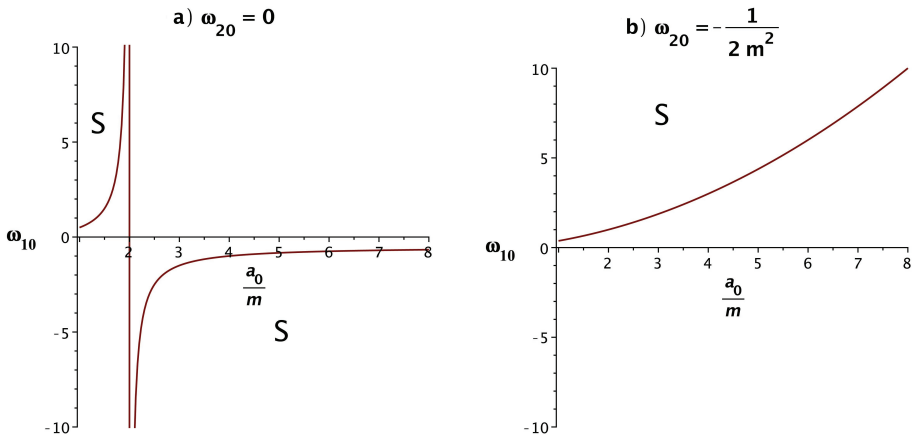

Figure 2.11: The stability diagram for a symmetric ERN TSW with a) the barotropic EoS and b) the variable EoS. As expected, the infinite discontinuity is removed due to the fine-tuning of the variable EoS.

$-0.4146553639/m^2$, and $\omega_{20}|_{b=1} = -0.4162095590/m^2$, the existed discontinuities will be removed. This can be seen clearly in Fig. 2.12, where the related mechanical stability diagrams are plotted for the three cases, once when $\omega_{20} = 0$ (barotropic EoS), and once when it is fine-tuned to remove the discontinuity. In all the subfigures, the horizontal axis starts at M/m, and the stable regions are marked with an "S". Note that a similar analysis can be applied to other admissible values of b and/or $|q|/m$.

In short, we identified the cause of the emergence of infinitely branching discontinuity, resembling a phase transition: they arise from the vanishing of the denominator of ω_{10} at equilibrium radius (Eq. (2.42)). In consequence, ω_{10}, which is expected to be finite, diverges. We showed how such divergences could be removed applying a different type of EoS. Finally, we have used asymmetric TSWs in the sense that the spacetimes on different sides of the throat differ only parametrically. Undoubtedly, the spacetimes that differ in r-dependence also can be considered within the range of application.

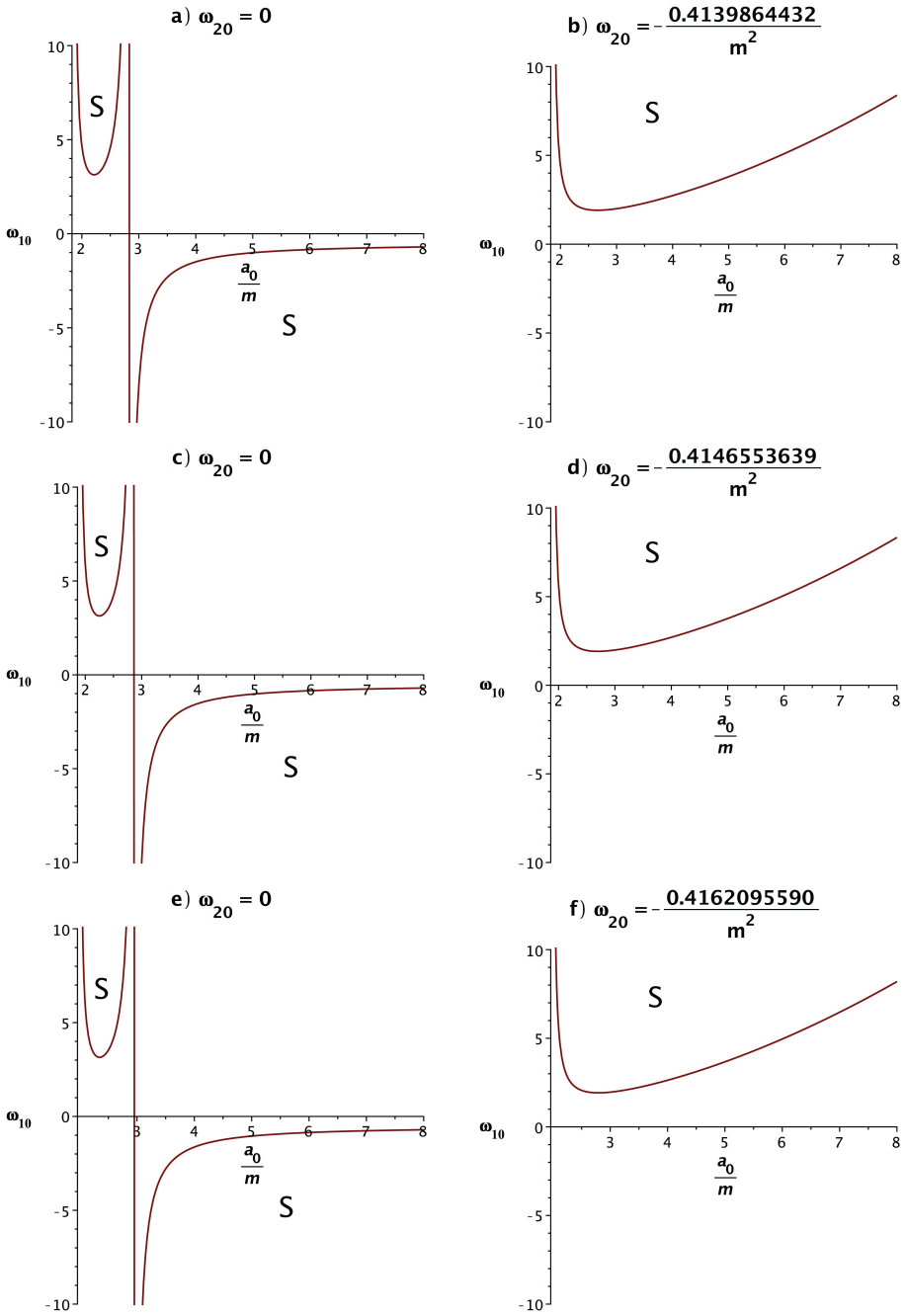

Figure 2.12: The stability diagram for a symmetric dilaton TSW for $a)$ $b = 0$ with a barotropic EoS, $b)$ $b = 0$ with a fine-tuned variable EoS, $c)$ $b = 0.5$ with a barotropic EoS, $d)$ $b = 0.5$ with a fine-tuned variable EoS, $e)$ $b = 1$ with a barotropic EoS, and $f)$ $b = 1$ with a fine-tuned variable EoS. The value of $|q|/m$ is set half for all the cases. The fine-tuned values of γ_0 are given at the top of each diagram. The regions with "S" are where the TSW is mechanically stable.

2.3 Construction of a Cylindrical ATSW

In this section we study the ATSWs constructed from cylindrically symmetric bulk spacetimes. The cylindrically symmetric spacetimes are one degree lower symmetric systems in comparison with the spherically symmetric ones. This can easily be visualized by comparing a cylinder and a sphere. In analogy, an axially symmetric space can also be categorized in a less symmetric configuration in comparison with the spherically symmetric ones. Rotation of a spherically symmetric spacetime is known to lose its spherical symmetry and it transforms into a stationary symmetric one. This is exactly how rotation transforms the Schwarzschild spacetime into the stationary Kerr spacetime. While cylindrically symmetric wormholes [109–116], cylindrically symmetric thin-shell wormholes (TSWs) [21, 24, 117–126] and asymmetric wormholes [87–89] have been considered in the literature, the absence of asymmetric thin-shell wormholes (ATSWs) was felt. Our aim in this section is to fill this void.

The main disadvantage of a cylindrical system is the occurrence of a non-compact direction, i.e. the $z-$axis, so that we cannot mention of an asymptotic flatness in such a spacetime. Only for a slice, say $z=$const., we can extend the radial coordinate to spatial infinity and discuss the asymptotic flatness in a restricted sense. The singularity structure of a cylindrically symmetric system is also different from a compact spherical system. Hereupon, one may face the question "with so much research on spherical TSWs, why to study the cylindrical TSWs?" First of all, cylindrical symmetry is the natural extension of spherical symmetry that we encounter in nature. For curiosity we want to know about cylindrical objects which are topologically related also with planar symmetric objects. Secondly, with their natural cylindrical symmetry, cosmic strings are shown not only to be involved in astronomical phenomena such as gravi-

tational lensing effect [127, 128], but also have roots in the foundation of large-scale structure of the universe [129], and correlations with the cosmic background radiation [130,131]. However, the validity of TSWs constructed by such spacetimes must be examined by constrains due to cosmological observations [67]. Thirdly, much interest arouse recently on collision of wormholes [132], in analogy with colliding black holes. Recall that detection of strong gravitational wave pulses at LIGO and Virgo [133, 134] are believed to arise as a result of black holes' mergers. Similar pulses are expected to emerge also from colliding wormholes. The existence of event horizon acts as a sink to absorb almost all radiation, leaving very little to escape and reach our planet Earth for detection. Since wormholes have no horizon, in case they undergo mutual collision/merger the resulting ring-down has more potential to reach us. Expectedly rotating black holes/wormholes carry more information through the polarization content of the radiated gravitational pulses. Cylindrical wormholes also are expected to yield ring-down, strong enough with its additional echo from the throat, that can be detected as cylindrical gravitational waves. It is well-known that the prototype form of cylindrical gravitational waves were proposed first by Einstein and Rosen [135]. Later on, these waves were generalized to cover the second polarization mode as well [136]. Detection of such cylindrical pulses will provide ample proof that they originate from cylindrically symmetric sources such as the surrounding of black holes and wormholes. Asymmetric TSWs considered in this dissertation will provide further feedback for cylindrical ring-down. For this reason, further research becomes inevitable to study the quasinormal modes (QNM) for the cylindrical TSW spacetimes. This particular study, of course, lies beyond the scope of the present project.

In what follows we apply the same approach as the previous section to, first construct,

and then study the stability of cylindrical ATSWs under a radial perturbation. Unlike the stability analysis of a localized spherical system, in a cylindrical system perturbation must be effective both in radial as well as in axial directions. In a simpler approach, however, we suppress the $z-$dependence and consider the metric functions depending only on the radial coordinate. This amounts to reflection symmetry in the $z-$direction by choosing a slice of constant $z-$surface.

Although we will start by establishing a generic framework, the sources of our spacetimes considered here will be a line source for the Levi-Civita (LC) metric with a cosmological constant Λ [137], which with the right selection of parameters can be reduced to a cosmic string (CS) [138] or a black string (BS) [139] metric. These are chosen deliberately, simple enough to expose the role of asymmetry in a cylindrical spacetime. Choosing different values of the parameters on different sides of the throat gives rise to asymmetry in the TSW. The next step is to address the stability analysis of an ATSW by assuming a generalized fluid EoS after the perturbation. Once a metric is perturbed, a new energy-momentum arises to counterbalance the nonzero curvature terms on the left-hand side of the Einstein equations. Similar to the previous section, we mostly intend to employ a variable EoS. However, whenever needed, we may go back to the barotropic EoS just by repealing the explicit radial-dependency of the pressure (by setting $\omega_{20} = 0$).

Although the steps to construct an ATSW out of cylindrically symmetric spacetimes is quite similar to the ones in the previous section, we prefer to start from scratch. This way, we ensure that small differences that naturally arise from the essential distinction between the cylindrical and spherical coordinates do not mislead. To establish

a framework which the spacetimes with cylindrical geometry in general relativity fit into, we begin by initiating the metrics of the two sides of the wormhole in their general diagonal cylindrically symmetric form as

$$ds_{\pm}^2 = -A_{\pm}(r_{\pm})\,dt_{\pm}^2 + B_{\pm}(r_{\pm})\,dr_{\pm}^2 + C_{\pm}(r_{\pm})d\phi_{\pm}^2 + D_{\pm}(r_{\pm})dz_{\pm}^2, \tag{2.58}$$

where the metric functions $A_{\pm}(r_{\pm})$, $B_{\pm}(r_{\pm})$, $C_{\pm}(r_{\pm})$ and $D_{\pm}(r_{\pm})$ are all positive functions of $r_{\pm}$. To construct the TSW by Visser's standard cut-and-paste procedure [7, 8], from each spacetime we cut a submanifold $(\Upsilon, g)^{\pm} = \{x_{\pm}^{\mu} | r_{\pm} \geq a(\tau) > r_{eh}\}$, and bring them together at $\mathcal{H} = \{x_{\pm}^{\mu} | r_{\pm} = a\}$, which is their common timelike hypersurface. By this, we connect the two spacetimes at their common boundary $\mathcal{H}$, the well-known throat of the wormhole. In case of absence of any horizon, i.e. for the non-black hole spacetimes, we excise out the singularity (if any) on the source of the string (both cosmic and black), which topologically gives rise to deficit/surplus angle.

The time-dependent equation defining $\mathcal{H}$ is implicitly given by Eq. (2.2) where τ is the proper time on the throat. Having the ATSW constructed, imposing the Darmois-Israel junction conditions [92, 93] on the metric and the curvature of the throat will be the next step. Firstly, these conditions give a unique metric on the TSW given by

$$ds_{\mathcal{H}}^2 = h_{ab}d\xi^a d\xi^b = -d\tau^2 + C(a(\tau))d\phi^2 + D(a(\tau))dz^2, \tag{2.59}$$

where $\xi^a = \{\tau, \phi, z\}$ are the local coordinates of the throat. Comparing Eq. (2.58) to Eq.(2.59) amounts to the counterparts of Eqs. (2.4a - 2.4c) as

$$\left[-A_{\pm}(r_{\pm})\,dt_{\pm}^2 + B_{\pm}(r_{\pm})\,dr_{\pm}^2\right]_{r_{\pm}=a(\tau)} = -d\tau^2, \tag{2.60a}$$

$$\begin{cases} C_{\pm}(r_{\pm})|_{r_{\pm}=a(\tau)} = C(a(\tau)) \\ D_{\pm}(r_{\pm})|_{r_{\pm}=a(\tau)} = D(a(\tau)) \end{cases}, \tag{2.60b}$$

and

$$\{\phi_{\pm}, z_{\pm}\} = \{\phi, z\}. \tag{2.60c}$$

At the throat, Eqs. (2.5a and 2.5b) hold, as well. Secondly, passing through the TSW from one side to the other, there is a jump in the extrinsic curvature tensor which indicates the presence of a matter field at the throat. This second condition is mathematically expressed by the Lanczos equations [91] given in Eq. (2.6). The energy-momentum tensor S_b^a belonging to the fluid localized on the throat is given by

$$S_b^a = diag\left(-\sigma, p_\phi, p_z\right), \tag{2.61}$$

where σ is the energy density, while p_ϕ and p_z are the lateral pressures of the fluid along ϕ and z, respectively.

In order to establish Eq. (2.6) explicitly for our general metrics, we begin by the definition of the components of the covariant extrinsic curvature tensor given in general by Eq. (2.7), where $x^\mu = \{t, r, \phi, z\}$ are the coordinates of the bulk spacetimes, and $\xi^b = \{\tau, \phi, z\}$ are the coordinates of the TSW. Having considered all these and the steps that amounted to Eqs. (2.17a and 2.17b), the Lanczos equations for the energy density and the pressures along ϕ and z amount to

$$\sigma = -\frac{(CD)'}{2CD} \sum_{i=+,-}^{2} \left(\sqrt{\frac{1+B_i\dot{a}^2}{B_i}} \right), \tag{2.62a}$$

$$p_\phi = \sum_{i=+,-} \sqrt{\frac{B_i}{1+B_i\dot{a}^2}} \left[\ddot{a} + \frac{(A_iB_iD)'}{2A_iB_iD}\dot{a}^2 + \frac{(A_iD)'}{2A_iB_iD} \right], \tag{2.62b}$$

and

$$p_z = \sum_{i=+,-} \sqrt{\frac{B_i}{1+B_i\dot{a}^2}} \left[\ddot{a} + \frac{(A_iB_iC)'}{2A_iB_iC}\dot{a}^2 + \frac{(A_iC)'}{2A_iB_iC} \right]. \tag{2.62c}$$

Herein, a prime and an overdot imply a total derivative with respect to the radius a and to the proper time τ, respectively.

Readjusting Eq. (2.62a) leads to an energy equation of type Eq. (2.20), with the radius-dependent effective potential being

$$V(a) = \frac{1}{2}\left(\frac{1}{B_+} + \frac{1}{B_-}\right) - \left[\frac{(CD)'}{4CD\sigma}\left(\frac{1}{B_+} - \frac{1}{B_-}\right)\right]^2 - \left[\frac{CD\sigma}{(CD)'}\right]^2. \tag{2.63}$$

The potential is then expanded using Taylor series about a hypothetical static equilibrium radius $a_0 > r_{eh}$ to a quadratic term as in Eq. (2.22). In this equation, the first two terms on the right-hand side are zero due to the static version of Eq. (2.20), and the assumption that a_0 is indeed the equilibrium radius, respectively. Therefore, in the very vicinity of a_0, the effective potential $V(a)$ is approximated by the first non-zero term on the right-hand side of Eq. (2.22), i.e. the third term which is proportional to $V''(a_0)$. If $V''(a_0) > 0$ ($V''(a_0) < 0$), the state of the ATSW is said to be mechanically stable (unstable). In order to proceed with the stability analysis, $V''(a_0)$ must be explicitly calculated, and an EoS is required to do so. The three expressions in Eqs. (2.62a - 2.62c) are not independent of each other and in fact are related by two generic variable EoSs $p_\phi = p_\phi(\sigma, a)$ and $p_z = p_z(\sigma, a)$. Finally, performing a covariant derivative on the energy-momentum tensor S^{ab} yields the counterpart of Eq. (2.18) as

$$\sigma' + \left[\frac{(CD)'}{CD} + \frac{C'D' - (CD)''}{(CD)'}\right]\sigma + \frac{1}{2}\left(\frac{C'}{C}p_\phi + \frac{D'}{D}p_z\right) = \frac{(CD)'}{4CD}\sum_{i=+,-}^{2}\left[\frac{(A_iB_i)'}{A_iB_i}\left(\sqrt{\frac{1+B_i\dot{a}^2}{B_i}}\right)\right]. \tag{2.64}$$

Given certain metrics, Eqs. ((2.62a - 2.62c) and their static counterparts, together with Eqs. (2.63) and (2.64) will be employed to construct the ATSW. As the subject matter, first we will have an overview on a rather general non-rotating metric in cylindrical coordinates which is known by different names; while some authors call it the Levi-Civita (LC) solutions with a non-zero cosmological constant (LCC or LCΛ) [140,141], some others call it the Linet-Tian (LT) metric [142, 143]. We will refer to it as the latter. If $\Omega > 0$ is the conicity of the spacetime, this metric for a negative cosmological constant has a general form of [144, 145]

$$ds^2 = dr^2 + Q(r)^{\frac{2}{3}} \left[-P(r)^{\frac{2\mu(\lambda)}{3\kappa(\lambda)}} dt^2 + \frac{1}{\Omega^2} P(r)^{\frac{2\nu(\lambda)}{3\kappa(\lambda)}} d\phi^2 + P(r)^{\frac{2\xi(\lambda)}{3\kappa(\lambda)}} dz^2 \right], \tag{2.65}$$

where the metric functions are given by

$$\begin{cases} Q(r) = \frac{\sinh\left(\sqrt{-3\Lambda} r\right)}{\sqrt{-3\Lambda}} \\ P(r) = \frac{2\tanh\left(\sqrt{-3\Lambda} r/2\right)}{\sqrt{-3\Lambda}} \end{cases}, \tag{2.66a}$$

which comprise the cosmological constant Λ. The other parameters are defined by

$$\begin{cases} \kappa(\lambda) = 4\lambda^2 - 2\lambda + 1 \\ \mu(\lambda) = -4\lambda^2 + 8\lambda - 1 \\ \nu(\lambda) = -4\lambda^2 - 4\lambda + 2 \\ \xi(\lambda) = 8\lambda^2 - 4\lambda - 1 \end{cases}, \tag{2.66b}$$

as functions of λ, a parameter related to the linear mass density of the source [140], satisfying the constraint $\mu(\lambda) + \nu(\lambda) + \xi(\lambda) = 0$. Due to the available symmetries [142], the conicity characteristics of the spacetime and the behavior of geodesics [141], the permitted domain of λ is $[0, 1/2]$ [143]. In order to have the LT metric with a positive cosmological constant, however, one substitutes the hyperbolic functions with their normal trigonometric counterparts, and $-\Lambda$ with Λ [141]. The metrics for either

positive or negative cosmological constant, recover the LC solution when $\Lambda \to 0$ [137]. Nevertheless, we intend to focus more on the LT metric with $\Lambda < 0$, because this metric has similar properties to anti-de Sitter (AdS) spacetime as $r \to \infty$ when λ is set to zero. This, however, does not mean that for $\lambda = 0$ we have exactly the AdS spacetime, because AdS, when is implemented in cylindrical coordinates, is not static [146]. This makes this case more realistic compared to either the LC solutions for $\Lambda = 0$ or the LT solutions with $\Lambda > 0$. It is also worth mentioning that the solutions in Eq. (2.65) are not singular anywhere in spacetime except at the axis $r = 0$. Note that even $r = 0$ is non-singular when $\lambda = 0$ or $\lambda = 1/2$ [141].

When it comes to an ATSW made by two non-identical LT universes (an LT ATSW), one must be sure that the conditions in Eq. (2.60b) are satisfied. In general, this explicitly means that the highly non-linear relations

$$\frac{1}{\Omega_1^2} Q(r,\Lambda_1)^{\frac{2}{3}} P(r,\Lambda_1)^{\frac{2\nu(\lambda_1)}{3\kappa(\lambda_1)}} = \frac{1}{\Omega_2^2} Q(r,\Lambda_2)^{\frac{2}{3}} P(r,\Lambda_2)^{\frac{2\nu(\lambda_2)}{3\kappa(\lambda_2)}} \tag{2.67a}$$

and

$$Q(r,\Lambda_1)^{\frac{2}{3}} P(r,\Lambda_1)^{\frac{2\xi(\lambda_1)}{3\kappa(\lambda_1)}} = Q(r,\Lambda_2)^{\frac{2}{3}} P(r,\Lambda_2)^{\frac{2\xi(\lambda_2)}{3\kappa(\lambda_2)}} \tag{2.67b}$$

must hold simultaneously. With the level of complexity the two equations above bring into the calculations, the stability analysis of the ATSW will practically be so challenging. Instead, we will choose particular metrics which are generated from the rather general LT metric under special conditions. Again, we emphasize that due to the conditions in Eq. (2.60b), not all the metrics that the LT metric covers can be subject to an ATSW study. For example, the LC metric itself cannot be examined within the ATSW context, because when the conditions $C_+(r_+)|_{r_+=a} = C_-(r_-)|_{r_-=a}$

and $D_+(r_+)|_{r_+=a} = D_-(r_-)|_{r_-=a}$ are satisfied for such a metric, the TSW cannot be asymmetric anymore. We now proceed with particular examples.

2.3.1 Stability of a Cosmic String ATSW

As it was discussed in the lines above, while $\Lambda \to 0$ in the LT metric evokes the LC solutions, $\lambda \to 0$ gives rise to the so-called non-uniform AdS metric [146]. However, combining these two limiting conditions leads to

$$ds_\pm^2 = -dt_\pm^2 + \Omega_\pm^2 d\rho_\pm^2 + \rho_\pm^2 d\phi_\pm^2 + dz_\pm^2, \tag{2.68}$$

for the two joined spacetimes, which are reparametrized with

$$\rho_\pm = \frac{r_\pm}{\Omega_\pm}. \tag{2.69}$$

This metric, which is a vacuum solution to the Einstein field equations, is identified by many names; "*the metric of a straight spinning string in cylindrical coordinates with parameter* $a = 0$" in [147], the cosmic string (CS) metric [138] or the Gott's solution [148]. A cosmic string geometry [149] is basically a spacetime warped by an infinitely long, straight and static massless cosmic string [150]. The spacetime has a conical singularity along the world sheet of the string, however, it is flat and smooth everywhere else. Comparing Eqs. (2.58) and (2.68) and recalling the condition in Eq.(2.60b), we see that on the throat it appoints

$$\begin{cases} A_\pm = 1 \\ B_\pm = \Omega_\pm^2 \\ C = a^2 \\ D = 1 \end{cases}. \tag{2.70}$$

Besides, we redefine $\Omega_{\pm}$ such that they are related to each other by an asymmetry factor ϵ, so that we can investigate our results based on the degree of asymmetry i.e. the value of ϵ. Hence, we set down $\Omega_{-} \equiv \Omega$ and $\Omega_{+} \equiv (1+\epsilon)\,\Omega$, where the domain of ϵ is seemingly $(-1,\infty)$. However, it is important to note that while for $\Omega_{\pm} > 1$ the spacetime has a conical geometry at t =const. and z =const. with angular defect $\delta_{\pm} = 2\pi\left(\frac{\Omega_{\pm}-1}{\Omega_{\pm}}\right)$, for $\Omega_{\pm} < 1$ there exists a surplus angle. Here we only consider deficit angle which implies $\Omega > 1$ and $(1+\epsilon)\,\Omega > 1$. Hence, the admissible domain of ϵ is instead $[0,\infty)$.

The energy conservation in Eq.(2.64) takes the following simple form

$$\sigma' + \frac{1}{a}\left(\sigma + p_{\phi}\right) = 0, \tag{2.71}$$

in which there is no wake of p_z, because the metric in every plane with t =const. and z =const. has the same geometry. Hence, the energy density and the angular pressure given by Eqs. ((2.62a - 2.62c), and their static counterparts reduce to

$$\sigma = -\frac{1}{a\Omega}\left[\sqrt{1+\Omega^2\dot{a}^2} + \frac{1}{1+\epsilon}\sqrt{1+(1+\epsilon)^2\,\Omega^2\dot{a}^2}\right], \tag{2.72a}$$

$$p_{\phi} = \ddot{a}\Omega\left[\frac{1}{\sqrt{1+\Omega^2\dot{a}^2}} + \frac{1+\epsilon}{\sqrt{1+(1+\epsilon)^2\,\Omega^2\dot{a}^2}}\right], \tag{2.72b}$$

and

$$\sigma_0 = -\frac{1}{a_0\Omega}\left(\frac{2+\epsilon}{1+\epsilon}\right), \tag{2.73a}$$

$$p_{\phi 0} = 0, \tag{2.73b}$$

respectively at the throat. These are in complete agreement with the results in [151].

Accordingly, for a CS ATSW, the expression for the effective potential in Eq. (2.63) will be

$$V(a) = -\left(\frac{\sigma a}{2}\right)^2 - \left[\frac{\epsilon(2+\epsilon)}{2\sigma(1+\epsilon)^2\Omega^2 a}\right]^2 + \frac{1+(1+\epsilon)^2}{2(1+\epsilon)^2\Omega^2}, \tag{2.74}$$

explicitly. To compute $V''(a_0)$, we need the first and the second derivatives of the energy density with respect to the radius. Thus, wherever needed, for the first derivative of the energy density σ' we substitute from Eq. (2.71) and for the second derivative we apply

$$\sigma'' = \frac{1}{a^2}\left(\sigma + p_\phi\right)(2+\omega_1) - \frac{\omega_2}{a}, \tag{2.75}$$

in which we have used $\omega_1 \equiv \partial p_\phi(\sigma, a)/\partial\sigma$ and $\omega_2 \equiv \partial p_\phi(\sigma, a)/\partial a$ in

$$p'_\phi = \frac{\partial p_\phi(\sigma, a)}{\partial a} + \frac{\partial p_\phi(\sigma, a)}{\partial\sigma}\sigma'. \tag{2.76}$$

Eventually, by replacing the radius a with a scaled radius $x = \sqrt{\Omega}a$ (and $x_0 = \sqrt{\Omega}a_0$) we calculate the second derivative of the potential at the equilibrium radius as

$$V''(x_0) = \frac{-2}{\Omega}\left[\frac{\omega_{10}}{(1+\epsilon)x_0^2} + \frac{\omega_{20}}{2+\epsilon}\right]. \tag{2.77}$$

Solving $V''(x_0) = 0$ for ω_{10} leads to

$$\omega_{10} = -\frac{(1+\epsilon)\omega_{20}x_0^2}{2+\epsilon}, \tag{2.78}$$

which is subject to the final analysis. It is straightforward to observe, that the angular pressure p_ϕ is either a function of both the radius a and the energy density σ, or of none. Therefore, a barotropic EoS cannot support a CS ATSW or a CS TSW, at least, in cylindrical coordinates. Additionally, according to the minus sign on the right-hand side of Eq. (2.78) the signs of ω_{10} and ω_{20} are reverse; a positive ω_{20} leads to a neg-

ative ω_{10} and vice versa. As it has been discussed in the previous sections, in fluid mechanics ω_{10} corresponds to the square of the speed of sound through the matter on the throat, and therefore, is physically meaningful in the interval $[0,1)$. However, due to the unusual (and unknown) characteristics of the exotic matter, ω_{10} might be corresponding to a whole different physical property and so exempted from the limitation $\omega_{10} \in [0,1)$. Nonetheless, if we somehow think of ω_{10} as the square of the speed sound in the exotic matter on the throat, then ω_{20} must firstly, be negative, and secondly, be adjusted such that we always have $\omega_{10} < 1$.

In Fig. 2.13, ω_{10} is plotted against $\omega_{20}x_0^2$ for different values of ϵ and the stable regions are marked. It is observed that by an increase in ϵ, the region of stability constantly shrinks (expands) for $\omega_{20} > 0$ ($\omega_{20} < 0$), meaning that for less symmetric ATSWs with higher asymmetry factors, there are less (more) pairs of $\left(\omega_{10}, \omega_{20}x_0^2\right)$ available such that the ATSW is mechanically stable. However, note that for the common stable regions, where the value of the second derivative of the effective potential at the throat ($V''(x_0)$ in Eq. (2.77)) is positive for all the admissible values of ϵ, the numerical value of $V''(x_0)$ is greater for a fixed ω_{10}, ω_{20} and x_0. To sum up, for positive (negative) values of ω_{20}, the more symmetric (asymmetric) the ATSW is, it has a better chance to be stable, although the stability of the symmetric TSW, corresponding to $\epsilon = 0$, is always stronger than the stability of an ATSW counterpart.

2.3.2 Stability of a Black String ATSW

Another interesting geometry can be constructed by setting $\lambda = \frac{1}{2}$ in Eq. (2.66b) [141]. In a set of new coordinates $(T, \rho, \varphi, \zeta)$, where

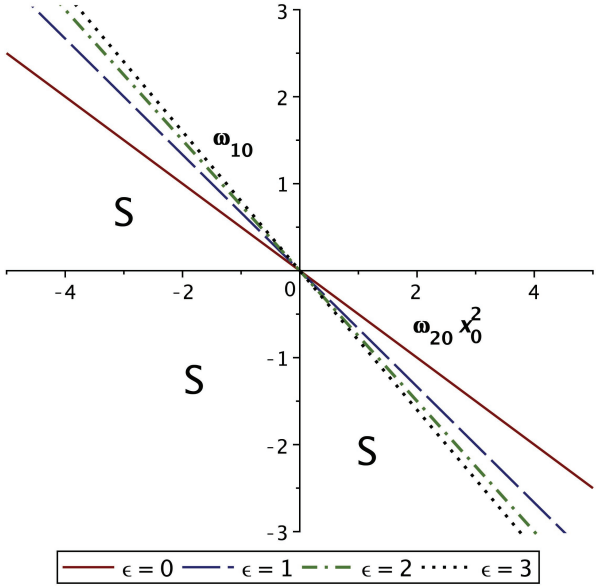

Figure 2.13: Stability regions of the CS ATSW visualized by plotting ω_{10} against $\omega_{20}x_0^2$ for various values of $\epsilon \in [0,\infty)$. The symmetric TSW corresponds to $\epsilon = 0$. For positive values of ω_{20} the probability of being stable increases by ϵ and vice versa.

$$\begin{cases} T = \frac{2\Omega}{-\Lambda}t \\ \rho = \frac{1}{\Omega}\cosh^{\frac{2}{3}}\left(\frac{\sqrt{-3\Lambda}r}{2}\right) \\ \varphi = \phi \\ \zeta = \Omega z \end{cases}, \tag{2.79}$$

the new line element, known by the name "*The uncharged, static black string metric*" [139, 152, 153], is given by

$$ds^2 = -\Psi(\rho)\,dT^2 + \frac{d\rho^2}{\Psi(\rho)} + \rho^2\left(d\varphi^2 + d\zeta^2\right). \tag{2.80a}$$

with the metric function

$$\Psi(\rho) = \alpha^2\rho^2 - \frac{4M}{\alpha\rho}. \tag{2.80b}$$

Herein, the parameter $\alpha^2 \equiv \frac{-\Lambda}{3}$, is positive definite and $M \equiv \frac{\alpha^3}{4\Omega^3}$ is associated with the linear mass density of the black string calculated at radial infinity [154]. This solution

is non-singular and has a horizon at $\rho_h = \frac{\sqrt[3]{4M}}{\alpha} = \frac{1}{\Omega}$. The metric function in Eq. (2.80b) could also be written as

$$\Psi(\rho) = \alpha^2\rho^2\left(1 - \frac{1}{\Omega^3\rho^3}\right). \tag{2.80c}$$

To investigate the stability of a BS ATSW, we require that the two spacetimes possess the same conicity (and so the same Ω) but different mass densities (and so different cosmological constants $\alpha_\pm$). Our stability method and steps will be analogous to the previous section.

Comparing Eqs. (2.58) and (2.80a), we observe that at the throat

$$\begin{cases} A_\pm = \Psi_\pm(a, \alpha_\pm) \\ B_\pm = \Psi_\pm^{-1}(a, \alpha_\pm) \\ C = D = a^2 \end{cases}, \tag{2.81}$$

where we require the cosmological constants to be related to each other by an asymmetry factor $\epsilon \in (-1, \infty)$, such that $\alpha_- \equiv \alpha$ and $\alpha_+ \equiv (1+\epsilon)\alpha$. Calculating for the energy conservation given in Eq. (2.64), one obtains

$$\sigma' + \frac{2}{a}(\sigma + p) = 0. \tag{2.82}$$

in which we have considered the fact that, according to Eqs. (2.62b and 2.62c), the angular and the axial pressures at the throat are equal, i.e. $p_\varphi = p_\zeta = p$. By applying Eqs. (2.62a, 2.62b) and (2.82), the energy density and the tangential pressure and their static equivalents are

$$\sigma = -\frac{2}{a}\left[\sqrt{\alpha^2a^2\left(1 - \frac{1}{\Omega^3a^3}\right) + \dot{a}^2} + \sqrt{(1+\epsilon)^2\alpha^2a^2\left(1 - \frac{1}{\Omega^3a^3}\right) + \dot{a}^2}\right], \tag{2.83a}$$

$$p=\frac{a\ddot{a}+\dot{a}^2+2\left(1+\epsilon\right)^2\alpha^2a^2\left(1-\frac{1}{4\Omega^3a^3}\right)}{a\sqrt{\left(1+\epsilon\right)^2\alpha^2a^2\left(1-\frac{1}{\Omega^3a^3}\right)+\dot{a}^2}}+\frac{a\ddot{a}+\dot{a}^2+2\alpha^2a^2\left(1-\frac{1}{4\Omega^3a^3}\right)}{a\sqrt{\alpha^2a^2\left(1-\frac{1}{\Omega^3a^3}\right)+\dot{a}^2}}, \quad (2.83b)$$

and

$$\sigma_0=-2\left(2+\epsilon\right)\alpha\sqrt{1-\frac{1}{\Omega^3a^3}}, \quad (2.84a)$$

$$p_0=\frac{2\left(2+\epsilon\right)\alpha\left(1-\frac{1}{4\Omega^3a^3}\right)}{\sqrt{1-\frac{1}{\Omega^3a^3}}}, \quad (2.84b)$$

respectively, which in turn lead to the radial potential

$$V\left(a\right)=\frac{1}{2}\left(\epsilon^2+2\epsilon+2\right)\alpha^2a^2\left(1-\frac{1}{\Omega^3a^3}\right) - \left[\frac{1}{\sigma}\epsilon\left(\epsilon+2\right)\alpha^2a\left(1-\frac{1}{\Omega^3a^3}\right)\right]^2-\left(\frac{\sigma a}{4}\right)^2. \quad (2.85)$$

Having this potential, one computes $V''(x_0)$, the second derivative of the potential at the rescaled equilibrium radius $x_0=\Omega a_0$, and from there, solving for $V''(x_0)=0$ one obtains an expression for ω_{10} in terms of x_0, ϵ, Ω, α and ω_{20} as

$$\omega_{10}=\frac{2\left(\epsilon+2\right)^2\left(x_0^3-1\right)}{3\Omega\left(\epsilon+1\right)}+\frac{3}{2\left(x_0^3-1\right)}-\frac{2\epsilon^2+3\epsilon+3}{2\left(\epsilon+1\right)}+\frac{2x_0^2\sqrt{x_0\left(x_0^3-1\right)}}{3\alpha\Omega\left(\epsilon+2\right)}\omega_{20} \quad (2.86)$$

Here ω_{10} and ω_{20} have the same definitions as in the previous section (Eq. (2.76)). To proceed further with Eq.(2.86) let us do some simplifications. Firstly, by $\Omega\to 1$ we assume that the deficit angle of both spacetimes is zero. Secondly, we consider a barotropic fluid at the throat. i.e. $\omega_{20}=0$. The results for ω_{10} against x_0 are plotted in Fig. 2.14 for different values of ϵ. All the values on the x_0-axis are beyond the rescaled event horizon $x_{eh}=1$. To determine which value of ϵ maximizes the area of the stability region, we took the following steps: Firstly, we calculated $S=\int_1^{\kappa}\omega_{10}dx_0$, where $\kappa>0$ is arbitrary. Secondly, we worked out $dS/d\epsilon=0$ to determine for which values of ϵ

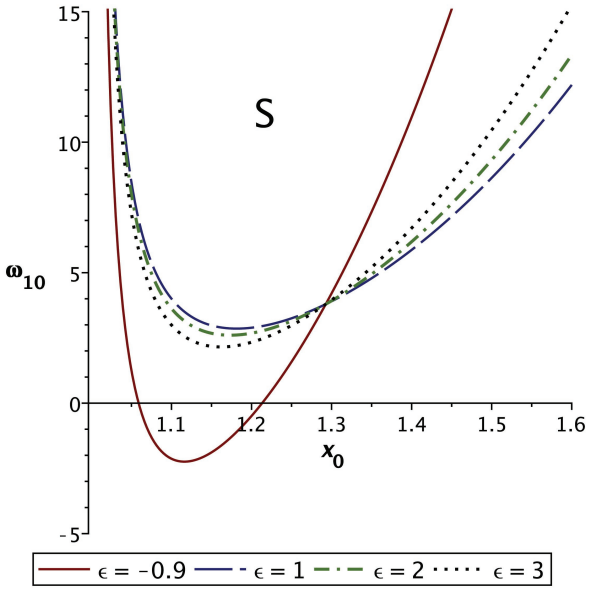

Figure 2.14: Stability region of the BS ATSW supported by a barotropic EoS with $\omega_{20} = 0$. The curves are drawn for various values of ϵ, including the symmetric TSW with $\epsilon = 0$ which has the most chance to be stable.

the surface area S is extremum. It is found out that the only extremum for admissible domain of ϵ occurs at zero. Next, learning that $d^2S/d\epsilon^2\big|_{\epsilon=0} > 0$ we concluded that $\epsilon = 0$ indeed leads to a minimum surface area under the curve in Fig. 2.14. Since the stability region is located above the curve, this means that when $\epsilon = 0$, and therefore the TSW is symmetric, the possibility of finding the TSW in a mechanically stable status is the greatest. However, this does not mean that $\epsilon = 0$ always leads to the most stable state. This can be seen from the explicit form of

$$V''(x_0) = -\frac{\alpha^2}{2x_0^3\left(x_0^3-1\right)}\Big[4(\epsilon+2)^2 x_0\left(x_0^3-1\right)^2 - 3\left(2\epsilon^2+2\epsilon\omega_{10}+2\omega_{10}+3\epsilon+3\right)\left(x_0^3-1\right)+9(\epsilon+1)\Big], \quad (2.87)$$

which is calculated for a barotropic fluid when $\Omega \to 1$. From Fig. 2.14 and Eq. (2.87) it can be perceived that for a fixed x and ω_{10}, $V''(x_0)$ may or may not exhibit a maximum for $\epsilon = 0$.

Chapter 3

ASYMMETRIC THIN-SHELL WORMHOLES IN NEW MASSIVE GRAVITY

3.1 Introduction

The mass of the quantum gravity's fundamental particle, the graviton, has been one of the most disputable subjects of modern physics. In massive theories of gravity, the spin-2 graviton is destined to move inside the local light cone, not on it. To point out the importance of massive theories of gravity let us draw a rough analogy with the Standard Model (SM) of particle physics by recalling that neutrino shared a similar history. In the SM, neutrino was also thought to be massless for a long time. With the advent of experimental neutrino physics, the picture has changed: neutrino has a very small but non-zero mass [155]. This amounts to changing much of the rules in the SM, leading even to revise a certain proportion of the textbooks. In analogy, with massive gravity, a certain revision in the fundamental physics of gravitational waves is expected. To prove the mass of a graviton, however, is more challenging than the neutrino. In the gravity side, even at a classical level, we had to wait until very recently when LIGO and Virgo detected gravitational waves from the merger of massive black holes in distant past [133,134]. Assuming that the gravity waves are massive, their speed in the vacuum will be less than the speed of light and this will naturally cause a delay in their arrival to the Earth. Nonetheless, an observation by LIGO and Virgo in 2017 put a constraint on this time delay, limiting the difference between the speed of gravitons and the speed of

photons to the interval $\left(-3\times10^{-15},+7\times10^{-16}\right)$-times the speed of light [134]. This means, that there still is an uncertainty in the mass of gravitons, and until the time the precision of our measurements lets us decisively confirm or reject the existence of massive gravitons, theoretical physics will keep contributing to the concept. See [156,157] as review studies, and references therein for more details on massive gravity.

In the literature, it was Fierz and Pauli who added a mass-dependent term to the gravity action for the first time in 1939 [158]. Since then, there have been so many attempts to establish a consistent quantum gravity theory, especially in 3+1 dimensions. However, most of these theories suffer from a common disadvantage: the absence of renormalizable theory. While renormalization is a big problem in 3+1 dimensions, things are different in 2+1. From simple power counting method of field theory, the lower dimension expectedly has natural advantages over the higher dimension [159]. Since 2+1-dimensional Weyl curvature vanishes identically, it is well-known that there are no pure gravitational degrees of freedom. For this reason, to create a theory, the source must be supplied in the lower dimension to make a gravitationally feasible theory. This is done by different methods, among which, two received more endorsements.

In an attempt to construct such a theory in 2+1 dimensions, Deser *et al.* established the theory of Topological Massive Gravity (TMG) in 1982 by adding a Chern-Simons term to the 3-dimensional Einstein-Hilbert (EH) action [160,161]. In 2009, Bergshoeff *et al.* suggested a different theory which later was known as New Massive Gravity (NMG) [162, 163]. This theory, which at the linearized level is the 2+1 dimensional equivalent of Pauli-Fierz theory, has the advantage over TMG that preserves parity symmetry [162–164]. Furthermore, it is shown in [165] and [166] that the theory is

unitary in tree level and renormalizable. However, it was shown later by Muneyuki and Ohta that the claim is wrong, and the unitarity and renormalizability are incompatible with each other [167]. de Rham *et al.* [168] go further to indicate that NMG is unitary even beyond the tree level. In [169] the authors prove that NMG at tree level is actually the only 3-dimensional unitary system which can be constructed by adding quadratic curvature terms to EH action. Add to all these remarkable characteristics, its invariance under general coordinate transformations is also manifest. NMG, therefore, gained much attention right after its introduction, for being a promising candidate for a renormalizable theory of quantum gravity. The theory also exhibits features like gravitational time dilation and time delay which the usual 3-dimensional general relativity is not subject to [169, 170]. Soon after the first publication, it was shown that NMG admits exact black hole solutions. In [171] warped AdS_3 black holes and $AdS_2 \times S^1$ solutions, in [163] Bañados-Teitelboim-Zanelli (BTZ) [172], new type black holes, and warped dS_3 and $dS_2 \times S^1$ solutions, in [173] extreme BTZ and a family of massive 'log' black holes, and in [173] and [174] AdS waves are discussed. Another important contribution is made by Oliva *et al.* who investigated exact black hole and non-black hole solutions of a special case with negative, positive and vanishing cosmological constant in [175]. Moreover, the Lifshitz metrics have been shown to be solutions of NMG for generic values of the dynamical exponent z (with an exact - asymptotically Lifshitz - black hole solution at $z = 3$) [176]. Ahmedov and Aliev, in a series of exquisite papers [177–179], discuss algebraic type D and type N solutions of NMG by employing a first-order Dirac-type differential operator. They indicate that the NMG field equations can be considered as the square of TMG field equations, and accordingly, argue the possibility of mapping all types D and N solutions of TMG into NMG. Besides,

they find new types D and N solutions in NMG with no counterparts in TMG. The stability of BTZ black holes in NMG are classically studied in [180]. Some of these aforementioned solutions will be considered here in this chapter.

Among all these, AdS_3 solutions are of greater importance for an obvious reason: Where there is a quantum-gravity consistent theory along with AdS solutions, there exists the AdS/CFT correspondence [181]. However, it was shown that on the boundary of the dual CFT, the unitarity of the AdS vacuum connotes a negative central charge [163,182]. Also, for logarithmic CFT correspondence (AdS_3/$LCFT_2$) see [183]. Setare and Kamali in [184] show that there is a perfect agreement between their results using 2-dimensional Galilean conformal algebra on the boundary of NMG with the Bekenstein-Hawking entropy (in the nonrelativistic limit) for warped AdS_3 and contracted BTZ black hole solutions of NMG. Phase transitions between BTZ black hole solutions and thermal solitons within NMG are studied in [185–187]. It is also worth mentioning that later, the new type black holes initially appeared in [163], came to the attention of Kwon *et al.,* who obtained their quasi-normal modes [188], and Gecim and Sucu, who studied the properties of relativistic spin-1/2 and spin-0 particles in this background [189]. NMG has also been generalized to 4th [190] and higher arbitrary dimensions [191]. Although, it is summed up in [166] that the higher dimensional generalizations are not unitary at the tree level.

Furthermore, there have been attempts to extend NMG. Among these, we point out the novel works by Güllü *et al.* [192, 193], which extend NMG to a 3-dimensional Born-Infeld theory of gravity (BI-NMG). There, the authors discuss that the cubic order extension of their augmented action duplicates the deformation of the NMG gained

from AdS/CFT correspondence. Exact black hole solutions of BI-NMG are discussed in [194], where properties such as mass, angular momentum, entropy and CFT dual central charges of the solutions are also determined. Extensions to higher curvature theories (R^3-NMG) and their exact solutions are considered in [195–198]. In [199] even higher derivative kinetic terms are discussed. Algebraic type N spacetime solutions to BI-NMG and their higher-order curvature corrections of NMG are studied in [200]. An extension of the theory by scalar matter with Higgs-like self-interaction is investigated in [201] with exact asymptotically dS_3 solutions which qualify as an eternally accelerated non-singular bounce-like 3D Universe. Another extension by scalar matter is discussed in [202], where the authors study a family of flat static domain walls as solutions. In [203], the NMG action is coupled to Maxwell's electromagnetic and Chern–Simons actions to give rise to charged black holes in both warped AdS_3 and log forms. Generalized Massive Gravity (GMG), whose action contains quadratic terms of both TMG and NMG along with coupling constants, and all its homogeneous solutions are studied in [204]. Exploiting the NMG action, a new bi-gravity model is constructed in 3 dimensions in [205]. Finally, a novel work by Dereli and Yetişmişoğlu suggests a model (new improved massive gravity (NIMG)) which includes TMG, NMG and minimal massive gravity (MMG) as subclasses of the theory [206, 207]. In this dissertation, we particularly consider the cosmological new massive gravity (CNMG) in 2+1-dimensions [163] and construct TSWs in such a theory.

In continuation, we choose a class of static solutions in CNMG and introduce the necessary junction conditions apt for a higher-order theory. This amounts to a revision of Darmois-Israel junction conditions that were designed for Einstein's general relativity [92, 93]. The qualified junction conditions in quadratic gravity are mentioned

in [208], and later in 2016, revised in [209]. It is worth mentioning that Eiroa *et al.* successfully applied the latter junction conditions to establish TSWs with a double layer [40], pure double-layer bubbles [210], and spherical thin-shells [211] in $F(R)$ theory of gravity.

3.2 Cosmological New Massive Gravity Solutions

The NMG theory is based on the $2+1$-dimensional cosmological new massive gravity (CNMG) action [163]

$$I_{\text{CNMG}} = \frac{1}{2\kappa}\int d^3x\sqrt{-g}\left(\varsigma R + \frac{1}{m^2}\left(R_{\mu\nu}R^{\mu\nu} - \frac{3}{8}R^2\right) - 2\lambda m^2\right), \tag{3.1}$$

in which κ^{-1} is the three dimensional reduced Planck mass, m is the mass of the graviton, $R_{\mu\nu}$ and R define the Ricci tensor and the Ricci scalar, respectively, and λ is a dimensionless cosmological parameter. The factor ς in Einstein-Hilbert term is merely a convention-dependent factor which takes on either 1 or -1.

In this study we consider the solutions of the theory which can be cast into the generic circularly symmetric form

$$ds^2 = -f(r)\,dt^2 + \frac{1}{f(r)}dr^2 + H^2(r)\,d\theta^2, \tag{3.2}$$

where

$$f(r) = c_0 + c_1 r + \frac{1}{2}c_2 r^2 \tag{3.3}$$

and $H(r)$ are functions of the radial coordinate r. Herein, c_0 and c_1 are integration constants to be interpreted as the mass parameter and gravitational hair of the given spacetime, respectively. The cosmological-like parameter c_2 can be reparametrized by

the cosmological parameter λ as

$$c_2 = 4m^2\left(\varsigma \pm \sqrt{1+\lambda}\right). \tag{3.4}$$

Setting $H(r) = r$ comprises BTZ, warped (A)dS$_3$ and new type black hole solutions, while setting $H(r) = 1$ recovers non-black hole (A)dS$_2\times$S^1 solutions. These are explained below in more details. Note that, in general, for $\lambda < -1$ there is no solution, and for $\lambda = 0$ the metric represents a flat spacetime.

$H(r) = r$: a) For $\lambda > -1$ we must have $c_1 = 0$. These solutions for $\varsigma = 1$ are locally isometric to AdS$_3$ and for $\varsigma = -1$ are locally isometric to dS$_3$. In the special case of $c_0 = 1$ one recovers (A)dS$_3$ vacua. Furthermore, in AdS$_3$ case $c_0 < 1$ admits static BTZ black holes with mass parameter $\mu = -c_0$. Also, for $\lambda = 0$ the solution is trivially flat.

b) For $\lambda = -1$ the solutions are called new type black holes. These special vacuum solutions for $\varsigma = 1$ ($c_2 > 0$) exhibit asymptotically AdS$_3$ unique vacua, while they are asymptotically dS$_3$ for $\varsigma = -1$ ($c_2 < 0$). In this case, the metric function $f(r)$, provided $c_1^2 - 8\varsigma m^2 c_0 \geq 0$, has a real double root at

$$r_{1,2} = \frac{1}{4m^2}\left(-\varsigma c_1 \pm \sqrt{c_1^2 - 8\varsigma m^2 c_0}\right). \tag{3.5}$$

In AdS$_3$ case, when $r_1 > 0$ we have an asymptotically AdS black hole with its horizon at $r = r_1$. There will also be an inner horizon at $r = r_2$ in case $r_2 > 0$. For dS$_3$, on the other hand, there potentially exist two horizons. When $r_1 > 0$, the surface $r = r_1$ is similar to the cosmological horizon of dS spacetime. If also $r_2 > 0$, we will have a black hole with an event horizon at $r = r_2$. In this case, the occurrence of double roots

implies that in between the roots, i.e. $r_2 < r < r_1$, the static spacetime remains static, whereas for $r < r_2$ and $r > r_1$ becomes dynamic with $t \longleftrightarrow r$.

$H(r) = 1$: For $\lambda = -1$ the metric is Kaluza-Klein (KK) type vacuum solution, i.e. locally isometric to $AdS_2 \times S^1$ when $\varsigma = 1$ ($c_2 > 0$) [171], and to $dS_2 \times S^1$ when $\varsigma = -1$ ($c_2 < 0$) [163]. Let us note that c_0 and c_1 are parameters of the solution, while c_2 is related to the essential parameters of the theory, m and λ.

3.3 Junction Conditions

Since the construction procedure of TSWs has been given extensively in the previous chapter, we shall abstain from going over the details again. Merely, the reader must bear in mind that although the cut-and-paste procedure works fine in NMG, the junction conditions are absolutely different from the ones in general relativity. In this section, we introduce two distinct sets of junction conditions, independently derived in [208] and [209] qualified for quadratic theories of gravity in arbitrary dimensions. In the latter, Reina, Senovilla and Vera (RSV) take advantage of the standard distributional analysis, while in the former, Deruelle, Sasaki and Sendouda (DSS) simplify the problem by using Gaussian coordinates at the joint hypersurface. In [209], RSV argue that using Gaussian coordinates often causes ignoring some important subtleties, and therefore, the reliability extent of the method is ambiguous (specially, when it comes to double layers). Nevertheless, since we are not considering double layers, for the sake of curiosity, we will apply both methods, independently, and count similarities and differences, if any. In what follows we particularly concentrate on timelike hypersurfaces which make more physical sense.

The junction conditions in [209] are derived to be applied to thin-shells. However, they

are also applicable to TSWs provided some slight modifications. The key difference between a thin-shell and a TSW stems from the selection of the normal vectors at the location of hypersurface. Each of the two spacetimes to be joined at the hypersurface has its own normal vector at the hypersurface. In a thin-shell, only one of the normal vectors is chosen (for instance the one going into $(\Sigma, g)^+$ and out of $(\Sigma, g)^-$), while for a TSW both normals are considered independently. Therefore, passing across the shell, the normal vector is continuous in thin-shells and discontinuous in TSWs. In TSWs, this distinction between normals is transmitted through all the extrinsic properties of the throat, since the normals play parts in them, by definition. Hence, one must be careful to hold the $(\pm)$ signs of the normals for a TSW, while they can be dropped casually for the case of a thin-shell. For the intrinsic properties (such as Riemann or Ricci tensors and Ricci scalar), of course, this does not apply.

3.3.1 TSW Construction with the RSV Junction Conditions

According to [209], a general quadratic Lagrangian density in $n+1$ dimensions has the form

$$\mathcal{L}_{\text{RSV}} = \sqrt{-g}\left(R + a_1 R^2 + a_2 R_{\mu\nu}R^{\mu\nu} + a_3 R_{\alpha\beta\mu\nu}R^{\alpha\beta\mu\nu} - 2\Lambda\right), \tag{3.6}$$

where a_n and Λ are constants with physical dimensions of $\left[L^2\right]$. A quick comparison with the CNMG action given in Eq. (3.1), reveals that $a_1 = \frac{-3\varsigma}{8m^2}$, $a_2 = \frac{\varsigma}{m^2}$ and $a_3 = 0$. Similar to the normal Israel junction conditions in general relativity, the diffeomorphism of the two spacetimes to be joined at the junction requires the first fundamental form to be continuous at their common hypersurface. This is the first junction condition and guarantees the identification of a global metric in the sense of distributions. To avoid non-physical distributional terms, in the case either a_2 or a_3 is nonzero, the

second junction conditions are identified as the continuity of the second fundamental form at the junction. There are also other junction conditions which basically insure that the other fundamental generalized functions are well-defined, as well. RSV also introduce the parameters $\kappa_1 = 2a_1 + a_2/2$ and $\kappa_2 = 2a_3 + a_2/2$ and classify their junction conditions in the case of a "*thin-shell without double layer*" based on the values of κ_2 and $n\kappa_1 + \kappa_2$. With regard to the coefficients a_1, a_2 and a_3, the proper conditions for $2+1$-dimensional NMG are the ones for the case "$\kappa_2 \neq 0$ *and* $n\kappa_1 + \kappa_2 = 0$". This is very interesting in the sense that even RSV would not think of this case as a serious one: "*Nevertheless, the relevance of this exceptional case is probably marginal, as the coupling constants satisfy a dimensionally dependent condition.*" [209]

In the literature of TSWs, the two spacetimes on the sides of the throat are traditionally considered to be exact copies of each other. However, it was shown in the previous chapter that this mirror symmetry can be broken by assigning different spacetimes to $(\Sigma, g)^{\pm}$, and develop ATSWs. We then follow the idea that this mirror symmetry is not a necessity in NMG, too. Therefore, the proper junction conditions for $n = 2$ are

$$\left[g_{\alpha\beta}\right]^{+}_{-} = 0; \tag{3.7a}$$

$$\left[K_{\alpha\beta}\right]^{+}_{-} = 0; \tag{3.7b}$$

$$\left[R_{\alpha\beta\mu\nu}\right]^{+}_{-} = \frac{[R]^{+}_{-}}{4}\left(n_\alpha n_\mu h_{\beta\nu} - n_\beta n_\mu h_{\alpha\nu} - n_\alpha n_\nu h_{\beta\mu} - n_\beta n_\nu h_{\alpha\mu}\right); \tag{3.7c}$$

$$\left[R_{\alpha\beta}\right]^{+}_{-} = \frac{[R]^{+}_{-}}{2}\left(\frac{1}{2}h_{\alpha\beta} + n_\alpha n_\beta\right); \tag{3.7d}$$

$$\left[\nabla_\mu R_{\alpha\beta}\right]^+_- = \left[n^\nu \nabla_\nu R_{\alpha\beta}\right]^+_- n_\mu + \frac{1}{2}\left(\frac{1}{2}h_{\alpha\beta} + n_\alpha n_\beta\right)\overline{\nabla}_\mu [R]^+_- - \frac{1}{4}[R]^+_-\left(n_\alpha K_{\beta\mu} + n_\beta K_{\alpha\mu}\right); \quad (3.7e)$$

$$S^\alpha_\alpha = 0; \quad (3.7f)$$

$$\kappa\left[S_{\alpha\beta}\right]^+_- = -(\kappa_1+\kappa_2)\left[RK_{\alpha\beta}\right]^+_- + \kappa_1\left[n^\nu\nabla_\nu R\right]^+_- + 2\kappa_2\delta^\rho_\alpha\delta^\sigma_\beta\left[n^\nu\nabla_\nu R_{\rho\sigma}\right]^+_-. \quad (3.7g)$$

(From [209], compare these with the associated junction conditions for thin-shells). Here, the S^α_α is the trace of the energy-momentum tensor of the shell, $S_{\alpha\beta}$, in its distribution form. Also, ∇ and $\overline{\nabla}$ are the covariant derivatives compatible with the metric g of the bulks and h of the shell, respectively. Furthermore, $[\Psi]^+_- \equiv \Psi^+ - \Psi^-$ denotes a jump in the function Ψ, passing across the thin-shell. Remark that, although all the indices are in Greek, for the quantities on the shell they only take on the coordinates on the shell, i.e. $\{t,\theta\}$. For the metric defined in Eq. (3.2) we calculate the nonzero independent components of Riemann and Ricci tensors, and Ricci scalar as follows

$$R_{trtr} = \frac{1}{2}f''; \quad (3.8a)$$

$$R_{t\theta t\theta} = \frac{1}{2}ff'HH'; \quad (3.8b)$$

$$R_{r\theta r\theta} = -\frac{H}{2f}\left(2fH'' + f'H'\right); \quad (3.8c)$$

$$R_{tt} = \frac{f}{2H}\left(f''H + f'H'\right); \quad (3.8d)$$

$$R_{rr} = -\frac{1}{2fh}\left(f'' + 2fH'' + f'H'\right); \quad (3.8e)$$

$$R_{\theta\theta} = -H\left(f'H' + fH''\right); \tag{3.8f}$$

$$R = -\frac{1}{H}\left(f''H + 2f'H' + 2fH''\right). \tag{3.8g}$$

Herein, a prime ($'$) denotes a total derivative with respect to the radial coordinate r. Imposing the first junction conditions (Eq. (3.7a)), necessitates

$$\begin{cases} f^{+}(a) = f^{-}(a) = f_a \\ H^{+}(a) = H^{-}(a) = H_a \end{cases}. \tag{3.9}$$

However, the second junction conditions (Eq. (3.7b)) compel a different result as

$$\begin{cases} f^{+\prime}(a) = -f^{-\prime}(a) \\ H^{+\prime}(a) = -H^{-\prime}(a) \end{cases}. \tag{3.10}$$

The jump in the Ricci scalar is a degree of freedom and considering Eqs. (3.8g), (3.9) and (3.10) is calculated as

$$[R]^{+}_{-} = \frac{1}{H_a}\left[H_a\left(f_a^{-\prime\prime} - f_a^{+\prime\prime}\right) + 2f\left(H_a^{-\prime\prime} - H_a^{+\prime\prime}\right)\right]. \tag{3.11}$$

However, it is convenient to construct the ATSW with two spacetimes with the same $H(r)$ functions on the sides. Hence, we require $H^{+}(r_{+}) = H^{-}(r_{-})$, which together with Eq. (3.10) admits

$$H^{+}(r_{+}) = H^{-}(r_{-}) = H_0, \tag{3.12}$$

where H_0 is an arbitrary constant. Accordingly, the second condition in Eq. (3.9) is also self-satisfied. With this assumption, exploiting Eq. (3.11) for $[R]^{+}_{-}$ and the junction conditions for Riemann tensor in Eq. (3.7c), result in

$$f^{+\prime\prime}(a) = f^{-\prime\prime}(a) = f''_a, \tag{3.13}$$

and consequently

$$[R]^{+}_{-} = 0. \tag{3.14}$$

While the junction conditions for the Ricci tensor components and their covariant derivatives (Eqs. (3.7d) and (3.7e)) are automatically satisfied, the condition for the trace of the energy-momentum tensor of the throat (Eq. (3.7f)) implies

$$\sigma = p. \tag{3.15}$$

This, of course, is nothing but the static equation of state (EoS) of the matter on the throat. Note that, for a perfect fluid on a $1+1$-hypersurface, the energy-momentum tensor is $S^{\beta}_{\alpha} = diag\,(-\sigma, p)$, with σ and p being the circumferential energy density and the angular pressure on the shell, respectively. Finally, the last of junction conditions (Eq. (3.7g)) give explicit terms for energy density and tangential pressure as

$$\sigma = \frac{3\varsigma}{4\kappa m^2}\sqrt{f_a}\left(f_a^{+\prime\prime\prime} + f_a^{-\prime\prime\prime}\right) \tag{3.16}$$

and

$$p = -\frac{\varsigma}{4\kappa m^2}\sqrt{f_a}\left(f_a^{+\prime\prime\prime} + f_a^{-\prime\prime\prime}\right), \tag{3.17}$$

respectively. However, simultaneous consideration of Eqs. (3.15), (3.16) and (3.17) suggests

$$f_a^{+\prime\prime\prime} = -f_a^{-\prime\prime\prime}, \tag{3.18}$$

which in turn leads to the static EoS

$$\sigma = p = 0. \tag{3.19}$$

Considering all the results above, imposes conditions on the metric function coefficients $c_1^{\pm}$ and $c_2^{\pm}$, as well as the radius of the ATSW, as follows

$$c_2^+ = c_2^-, \tag{3.20}$$

$$c_1^- = -c_1^+ - 2c_2^+ a, \tag{3.21}$$

and

$$a = \frac{-c_1^+ \pm \sqrt{c_1^{+2} - 2c_2^+ \left(c_0^+ - c_0^-\right)}}{2c_2^+} = \frac{-c_1^- \pm \sqrt{c_1^{-2} - 2c_2^- \left(c_0^- - c_0^+\right)}}{2c_2^-}, \tag{3.22}$$

respectively. Obviously, the radius is real only for $c_1^{+2} - 2c_2^+ \left(c_0^+ - c_0^-\right) \geq 0$. The TSW radius for the maximally symmetric case $c_0^+ = c_0^-$ amounts to the non-trivial result

$$a = -\frac{c_1^+}{c_2^+} = -\frac{c_1^-}{c_2^-}, \tag{3.23}$$

which is positive only when $c_1^{\pm}$ and $c_2^{\pm}$ have different signs. Since $c_2^+ = c_2^-$ this alludes $c_1^+ = c_1^-$, and the TSW is symmetric. For $H(r) = 1$ and $\lambda = -1$ this explicitly becomes

$$a = -\frac{c_1}{4\varsigma m^2}. \tag{3.24}$$

This is a strong condition which dictates on the radius of the TSW. Note that the signs of the parameters included must eventually be set such that $a > 0$. Depending on the sign of the quadratic term in the metric function f, this can be the maximum or the minimum of f. Here we emphasize that one may consider both possibilities $m^2 > 0$ and $m^2 < 0$, because the plus sign behind the quadratic terms in the CNMG action in Eq. (3.1) is more of a convention.

The above results imply, that firstly, the TSW is generally an asymmetric one, except

for the maximally symmetric case where $c_0^+ = c_0^-$, $c_1^+ = c_1^-$ and $c_2^+ = c_2^-$, and secondly, depending on the values of the metric coefficients, the TSW's radius can actually be real and positive. Providing the tuned up coefficients support the TSW's existence, it will have null energy density and pressure on its throat, providing a vacuum condition. Unexpected as it is, now the TSW indeed satisfies all the energy conditions. This represents a natural wormhole [212] with no matter on its throat. The two spacetimes are joined smoothly and the result is a complete Riemannian manifold with no exotic matter, no discontinuity or singularity of any sort.

3.3.2 TSW Construction with the DSS Junction Conditions

In [208] DSS have investigated the junction conditions for the quadratic Lagrangian density

$$\mathcal{L}_{\rm DSS} = \sqrt{-g}\left(R - 2\Lambda - 4\beta R_{\mu\nu}R^{\mu\nu} + \alpha R^2\right), \tag{3.25}$$

where α and β are two free parameters and Λ resembles a "bare" cosmological constant. To do so, they considered the Gaussian-normal coordinates to express the bulk metrics as

$$ds^2 = dy^2 + h_{ij}dx^i dx^j, \tag{3.26}$$

in which there exists a thin-shell located at $y = 0$, and h_{ij} represents the metric tensor of the 2-dimensional sub-spacetime. The proper junction conditions are found to be

$$4\left[-\beta\mathcal{H}_{ij} + (\alpha - \beta)\, h_{ij}\mathcal{H}\right]_-^+ = S_{ij} \tag{3.27}$$

where

$$\mathcal{H}_{ij} \equiv -\frac{1}{2}\frac{\partial^3 h_{ij}}{\partial y^3}, \tag{3.28}$$

$$\mathcal{H} \equiv h^{ij}\mathcal{H}_{ij}, \tag{3.29}$$

and S_{ij} is the total energy-momentum tensor on the shell.

With a brief comparison between the Lagrangian density of Eq. (3.25) and the action of CNMG given in Eq. (3.1), one finds $\alpha = -\frac{3\varsigma}{8m^2}$, $\beta = -\frac{\varsigma}{4m^2}$, and of course $\Lambda = \varsigma\lambda m^2$. Therefore, the junction conditions for CNMG can be written as

$$\frac{\varsigma}{m^2}\left[\mathcal{H}_i^{\ j} - \frac{1}{2}\delta_i^j\mathcal{H}\right]_-^+ = S_i^j. \tag{3.30a}$$

However, note that prior to checking for the conditions in Eq. (3.30a) one must check for the continuity of the metric, and its first and second derivatives with respect to the normal coordinate y at the shell's position; i.e. we must have

$$\left[h_{ij}\right]_-^+ = 0, \tag{3.30b}$$

$$\left[\frac{\partial h_{ij}}{\partial y}\right]_-^+ = 0, \tag{3.30c}$$

and

$$\left[\frac{\partial^2 h_{ij}}{\partial y^2}\right]_-^+ = 0. \tag{3.30d}$$

The conditions in Eq. (3.30a) can explicitly be determined as

$$\sigma = p = \frac{\varsigma}{2m^2}\left[\mathcal{H}_\theta^\theta - \mathcal{H}_t^t\right]_-^+. \tag{3.31}$$

Comparing the bulk metrics in Eqs. (3.2) and (3.26) admits

$$dy^2 = \frac{1}{f}dr^2 \tag{3.32}$$

and so

$$\frac{dr}{dy} = \sqrt{f}. \tag{3.33}$$

This also casts the metric of the TSW as

$$h_{ij}dx^i dx^j = -f dt^2 + H^2 d\theta^2. \tag{3.34}$$

For a general ATSW at $r = a$ (where $r_2 < a < r_1$ in case $\varsigma = -1$, and $r_1 < a$ in case $\varsigma = 1$), the last three junction conditions give rise to the exact same results as the previous section's for the metric functions and their derivatives as

$$H^+(r_+) = H^-(r_-) = H_0, \tag{3.35}$$

$$f^+(a) = f^-(a) = f_a\ , \tag{3.36}$$

$$f^{+\prime}(a) = -f^{-\prime}(a), \tag{3.37}$$

and

$$f^{+\prime\prime}(a) = f^{-\prime\prime}(a) = f_a'', \tag{3.38}$$

if again the rather physical assumption $H^+(r_+) = H^-(r_-)$ holds. Note that, each time that a derivative with respect to the Gaussian normal coordinate y is taken, the discontinuity in the normal vector to the throat must be considered, which emerges as the minus sign in the right-hand-side of Eq. (3.37). So far, it has been cleared up that only for the special choice $H(r) = 1$ the TSW can be constructed, and the circumstances and discussions after Eq. (3.24) in the previous section are also valid

here. Finally, the original junction conditions in Eq. (3.30a) and the explicit form

$$\mathcal{H}_{ij} = -\frac{1}{2}\left(\left(\left(\frac{\partial h_{ij}}{\partial r}\right)\sqrt{f}\right)'\sqrt{f}\right)'\sqrt{f} \tag{3.39}$$

impose

$$\sigma = p = 0, \tag{3.40}$$

which is in full agreement with the previous results.

It appears to us, that using DSS junction conditions, the same analysis can be applied to a wider range of massive quadratic Lagrangian densities and their solutions. To clear things up, let us consider a massive Lagrangian density of the form

$$\mathcal{L} = \sqrt{-g}\left(\varsigma R + \frac{1}{m^2}\left(R_{\mu\nu}R^{\mu\nu} + \gamma R^2\right) - 2\Lambda\right). \tag{3.41}$$

Any solution to this Lagrangian density with the form in Eq. (3.2) with $H(r) = r$, to be used to construct a TSW, will suffer from a discontinuity in the first derivative of the angular component of the TSW metric. Hence, the natural unsatisfactory behavior of such solutions to the junction conditions affects the occurrence of TSW, as if it had never existed.

On the contrary, solutions of the same type with $H(r) = 1$ satisfy all the boundary conditions, but identically lead to

$$\sigma = p = 0. \tag{3.42}$$

The same analysis, however, is not applicable to RSV junction conditions, since for a general quadratic Lagrangian density such as the one in Eq. (3.41), the value of

coefficient γ alters the junction conditions accordingly.

In conclusion, we found TSWs within CNMG which can be stable, but come to exist only when are asymmetric, in the sense that the bulk spacetimes on the two sides are different in geometry and nature. The tidbit is that for the cases we have studied here, such ATSWs do not need matter (neither ordinary nor exotic) as support, and hence, provide a smooth passage from one universe to the other.

Chapter 4

CONCLUSION

Wormholes spacetimes were discovered in the early decades of general relativity as exact solutions to the Einstein field equations. However, they suffered from two main drawbacks: firstly they were not traversable, in general, and secondly they demanded the existence of an unknown kind of matter. This so-called *exotic matter* does not satisfy the known energy conditions such as the weak energy condition. It took some decades until the late 1980s when Morris and Thorne addressed the first problem by systematically discussing the traversability of such wormholes and introduced a practically traversable wormhole. Soon afterward, Visser moderated the second problem by establishing the theory of thin-shell wormholes (TSWs). This new class of traversable wormholes had this advantage that confined the exotic matter to a thin-shell, i.e. the throat of the TSW. Furthermore, by applying Visser's method, called cut-and-paste technique, one is able to construct TSWs out of non-wormhole spacetimes such as Minkowski, Schwarzschild, ERN, dS and AdS spacetimes. As another advantage, in mid-1990s Poisson and Visser developed a method to study the stability of such wormholes by radially disturbing their throats. This linear stability analysis soon became so popular that many articles were published in the next two decades using the same method, with different spacetimes. The TSW studies also have found their way to higher dimensions and modified theories of gravity. However, in almost all the studies prior to this study, the structures of the TSWs had a mirror symmetry.

By this study, we have broken this mirror symmetry for the first time, by assigning to the side-spacetimes two geometries of a kind with different parameters (e.g. two Schwarzschild spacetimes with different central masses), or two geometries of different natures (e.g. a Schwarzschild spacetime and an ERN spacetime). This has been the main target of this study: to introduce Asymmetric Thins-Shell Wormhole as a new concept in the literature of traversable wormholes. Also, it was shown that the stability of such peculiar objects can be studied in the context of linear stability analysis. In chapter 2, we have worked this out for spherical and cylindrical solutions of general relativity, within a generic framework. Particularly, after constructing the ATSW and from the junction conditions, we derived the energy and pressure expressions, in accord with a variable EoS for a fluid at the throat. The radius of the throat is made dynamic by a linear, radial perturbation to study the consequences. The effective potential of the problem expectedly had a more intricate structure compared with the symmetric TSWs. Two critical parameters, $\omega_1 \equiv \partial p(\sigma, a)/\partial\sigma$ and $\omega_2 \equiv \partial p(\sigma, a)/\partial a$, are introduced and analyzed for each given source in connection with the effective potential.

In section 2.1, we studied special cases of a CoS ATSW with different geometrical parameters (section 2.1.1), a Schwarzschild ATSW with different masses (section 2.1.2), an ERN ATSW (section 2.1.3), a Schwarzschild-ERN ATSW (section 2.1.4), and an AdS-dS ATSW (section 2.1.5). We qualitatively examined their stabilities under various conditions, compared them with each other, and counted some similarities and differences with the special cases of symmetric thin-shell wormholes. Most importantly, in general, asymmetric structures of TSWs are less likely to be stable compared with the symmetric configurations. In fact, the more the asymmetry factor admits the

less chance to be stable. By this, it is meant that the regions of stability tend to shrink with the degree of asymmetry. Furthermore, for a barometric EoS, the stability diagrams maintain their generic shapes, consisting of a bowl-like branch followed by an asymptotically zero-seeking branch.

In section 2.2, we addressed an anomaly which appeared in the stability diagram of ATSWs with a barotropic fluid. The emergence of infinitely branching discontinuity, resembling a phase transition, seemed peculiar enough to attract attention since the stability analyses for TSWs were incepted. The prototype example was the Schwarzschild TSW, which had a similar discontinuity at the stability radius $a_0 = 3m$, as pointed out by Poisson and Visser [10]. In analogy, other TSWs also exhibited similar behavior. We identified the cause of such type of discontinuities: they arise from the vanishing of $-\left(C_0'/C_0\right)(\sigma_0 + p_0) + \left(2C_0C_0'' - C_0'^2\right)\sigma_0/2C_0C_0'$ at equilibrium radius (Eq. (2.42)). In consequence, the speed of sound ω_{10}, which is inversely proportional to this expression, and is expected to be finite, subsequently diverges. In an attempt to resolve such a discontinuity in the symmetric Schwarzschild TSW, Varela employs a more general, modified EoS, i.e. the variable EoS, to replace its barotropic counterpart [22]. In this rather general EoS, beside the energy density σ, the pressure p also depends on the radius of the shell which creates an extra degree of freedom to be used as an advantage. We have precisely shown that such a generalization can be systematically applied to all the TSWs, by pointing out to the reason of the emergence of the discontinuities. Our investigation is generalized to all spherically symmetric spacetimes, with the generic line element in Eq. (2.1), including non-asymptotically flat ones such as the dilaton TSW. This shows that the method is applicable even to those TSWs which are strongly coupled with the non-linear, non-asymptotically flat, dilatonic bulk spacetimes. In sec-

tion 2.2.1, the logic was illustrated by representing three examples (see Fig. 2.9 for the Schwarzschild TSW, Fig. 2.11 for ERN TSW and Fig. 2.12 for the dilaton TSW), where consequently, the discontinuities in question have been eliminated. It is not difficult to anticipate that the same technique could be applied to other TSWs as well, including the ones in alternative theories.

In section 2.3, Within the generic formalism, we have introduced classes of ATSWs in cylindrical coordinates which are essentially less symmetric than their spherical counterparts in previous sections. As a result, the equality of the spherical angular pressures, $p_\theta = p_\varphi$, split into different components p_φ and p_z in the cylindrical coordinates. The occurrence of non-equal pressures naturally makes the problem more difficult, which is simplified to certain extend by relying only on the radial type of perturbations in the stability analysis. The founded generic formalism in section was applied to the ATSW constructed by the LT bulk spacetime with three distinguishable parameters Ω, Λ and λ. To find a way out of the high level of complexity caused by the nature of the LT metric and the conditions the study is subject to, we narrowed down the case studies to two special metrics generated by the LT metric under certain selections of its parameters; the CS metric (section 2.3.1) and the BS metric (section 2.3.2). The CS ATSW was established by imposing an asymmetry in the values of their joined universes' conicities $\Omega_\pm$. The BS ATSW, on the other hand, was constructed by requiring an asymmetry in the values of the mass densities $M_\pm$ of the two spacetimes. The mass density of a BS universe is directly related to the conicity and cosmological constant of the universe through $M_\pm = \left(-\Lambda_\pm/3\right)^{3/2}/\left(4\Omega_\pm\right)$. To avoid unnecessary complication, we demanded the conicities of the two spacetimes to be the same, which immediately results in an asymmetry in the cosmological constants. The overall effect

is that, the real importance lies within the way the asymmetry is imposed; the value of the asymmetric factor ϵ.

Both intuitively and from the experience we gained in sections 2.1 and 2.2 with the spherical ATSWs, we expected the maximum probability of stability of cylindrical ATSWs to coincide with their degree of symmetries, in proportion. Except for a marginal case, it turned out that, this is also true for the cylindrical ATSWs we studied here. More detailed, we observed that in a CS ATSW with $\omega_{20} > 0$ (Fig. 2.12), and also in a BS ATSW (Fig. 2.13), any diversion from $\epsilon = 0$ decreases the chance of stability. The only exception is when $\omega_{20} < 0$ in a CS ATSW. We recall that the symmetric TSW corresponds to $\epsilon = 0$. Explaining this exceptional case demands a phenomenological study over the microphysical properties of the exotic matter, which is beyond the scope of this dissertation.

In chapter 3, we moved on to a modified theory of gravity, CNMG, to investigate the construction of ATSWs there. Earlier, we mentioned that it has been a long-standing challenge to obtain TSWs with physical, i.e. non-exotic matter in Einstein's general relativity. This was overcome in the past in particular models by changing the topology of the shell from spherical (in 3+1-dimensions) [80] and from circular (2+1-dimensions) forms [79, 81]. Giving up those symmetric topologies, however, gave rise to different problems in connection with their stability analysis. In chapter 3 we have shown that the exotic matter problem is overcome for TSWs in CNMG. In the meantime, the junction conditions are modified and they are distinct from those of Einstein's general relativity, i.e. the Darmois-Israel junction conditions. The new junction conditions are redefined and applied to some static solutions of CNMG. Our results show

no indications of major difference between the two distinct sets of junction conditions we have used independently. However, this is mostly for the quadratic nature of the metric function $f(r)$, and the specific selection of the gauge function $H(r)$. This can be seen the best in the structural differences between the expressions found for σ and p in Eqs. (3.16) and (3.17) using RSV junction conditions, and Eq. (3.31) using DSS junction conditions. More noticeably, the exotic matter nightmare gets resolved for TSWs in this theory, in the sense that the energy density and lateral pressure on the shell become zero (better than negative!), hence no known energy condition is violated anymore. Nevertheless, these TSWs could only be constructed for the gauge selection $H(r) = 1$. It was observed that for $H(r) = r$, which specifically comprises AdS solutions, no TSWs can be established. The existed TSWs, however, could be symmetric as well as asymmetric. We leave the profound question of "how these for AdS bulk translates into its CFT correspondence" for further studies. As a next step, investigating TSWs' constructions under naturally different geometries, such as Lifshitz black holes [176], is in order. Studying thin-shells with double layers may also be of interest, as for these ones demand some other junction conditions [209]. As another subject for further studies one may have a look into extended theories of NMG and solutions therein [192–207]

Three scientific articles are published from this dissertation [213–215]. In [213] spherically symmetric ATSWs in general relativity, in [214] the infinite discontinuity problem, and in [215] TSWs as well as thin-shells in NMG are considered. Furthermore, fate of an ATSW powered by a Morris-Thorne wormhole, and thermodynamic stability of a Schwarzschild TSW are studied in [216] and [217], respectively. Although the two latter papers are directly related to the topic of the thesis, we did not brought

the results here. Moreover, an article regarding the cylindrically symmetric ATSWs in general relativity [218] has been under review by a scientific journal at the time of publication of this thesis. .

REFERENCES

[1] L. Flamm, Physikalische Zeitschrift **1**, 448 (1916).

[2] A. Einstein, and N. Rosen, Phys. Rev. **48**, 73 (1935).

[3] M. S. Morris, and K. S. Thorne, Am. J. Phys. **56**, 395 (1988).

[4] M. S. Morris, and K. S. Thorne, U. Yurtsever, Phys. Rev. Lett. **61**, 1446 (1988).

[5] M. Azreg-Aïnou, J. Cosmol. Astropart. Phys. **07**, 037 (2015).

[6] M. Visser, *Lorentzian wormholes from Einstein to Hawking* (American Institute of Physics, New York, 1995).

[7] M. Visser, Phys. Rev. D **39**, 3182 (1989).

[8] M. Visser, Nucl. Phys. H **328**, 203 (1989).

[9] P.R. Brady, J. Louko, and E. Poisson, Phys. Rev. D **44**, 1891 (1991).

[10] E. Poisson, M. Visser, Phys. Rev. D **52**, 7318 (1995).

[11] S. W. Kim, Phys. Lett. A **166**, 13 (1992).

[12] J. P. S. Lemos, and F. S. N. Lobo, Phys. Rev. D **69**, 104007 (2004).

[13] F. Rahaman, M. Kalam, and S. Chakraborty, Gen. Relativ. Gravit. **38**, 1687 (2006).

[14] F. Rahaman, M. Kalam, and S. Chakraborty, Int. J. Mod. Phys. D **16**, 1669 (2007).

[15] F. Rahaman, M. Kalam, K. A. Rahman, and S. Chakraborty, Gen. Relativ. Gravit. **39**, 945 (2007).

[16] C. Bejarano, E. F. Eiroa, and C. Simeone, Phys. Rev. D **75**, 027501 (2007).

[17] E. Gravanis, and S. Willison, Phys. Rev. D **75**, 084025 (2007).

[18] M. G. Richarte, and C. Simeone, Int. J. Mod. Phys. D **17**, 1179 (2008).

[19] M. Halilsoy, A. Övgün, and S. H. Mazharimousavi, Eur. Phys. J. C **74**, 2796 (2014).

[20] A. Övgün, Eur. Phys. J. Plus **131**, 389 (2016).

[21] E. F. Eiroa, and C. Simeone, Phys. Rev. D **70**, 044008 (2004).

[22] V. Varela, Phys. Rev. D **92**, 044002 (2015).

[23] M. G. Richarte, I. G. Salako, J. P. Morais Graca *et al.*, Phys. Rev. D **96**, 084022 (2017).

[24] M. Sharif, and Z. Yousaf, Astrophys. Space Sci. **351**, 351 (2014).

[25] M. Sharif and M. Azam, Eur. Phys. J. C **73**, 2554 (2013).

[26] M. Thibeault, C. Simeone, and E. F. Eiroa, Gen. Relativ. Gravit. **38**, 1593 (2006).

[27] F. S. N. Lobo, and P. Crawford, Class. Quantum Grav. **21**, 391 (2004).

[28] E. F. Eiroa and G. E. Romero, Gen. Rel. Gravit. **36**, 651 (2004).

[29] S. H. Mazharimousavi, M. Halilsoy, and Z. Amirabi, Phys. Rev. D **89**, 084003 (2014).

[30] G. A. S. Dias, and J. P. S. Lemos, Phys. Rev. D **82**, 084023 (2010).

[31] E. F. Eiroa, Phys. Rev. D **78**, 024018 (2008).

[32] N. M. Garcia, F. S. N. Lobo, and M. Visser, Phys. Rev. D **86**, 044026 (2012).

[33] M. Ishak, and K. Lake, Phys. Rev. D **65**, 044011 (2002).

[34] E. F. Eiroa, and C. Simeone, Phys. Rev. D **83**, 104009 (2011).

[35] F. S. N. Lobo, and P. Crawford, Class. Quantum Grav. **22**, 4869 (2005).

[36] S. M. C. V. Gonçalves, Phys. Rev. D **66**, 084021 (2002).

[37] C. Bejarano, and E. F. Eiroa, Phys. Rev. D **84**, 064043 (2011).

[38] M. Sharif, and M. Azam, J. Cosmol. Astropart. Phys. **05**, 025 (2013).

[39] Z. Amirabi, M. Halilsoy, and S. H. Mazharimousavi, Phys. Rev. D **88**, 124023 (2013).

[40] E. F. Eiroa, and G.F. Aguirre, Phys. Rev. D **94**, 044016 (2016).

[41] E. F. Eiroa, and G.F. Aguirre, Eur. Phys. J. C **76**, 132 (2016).

[42] M.R. Mehdizadeh, M.K. Zangeneh, and F.S.N. Lobo, Phys. Rev. D **92**, 044022 (2015).

[43] T. Kokubu, T. Harada, Class. Quantum Gravity **32**, 205001 (2015).

[44] M. H. Dehghani, and M.R. Mehdizadeh, Phys. Rev. D **85**, 024024 (2012).

[45] X. Yue, and S. Gao, Phys. Lett. A **375**, 2193 (2011).

[46] A. Banerjee, K. Jusufi, and S. Bahamonde, Gravit. Cosmol. **24**, 1 (2018).

[47] S.V. Sushkov, Phys. Rev. D **71**, 043520 (2005).

[48] M. Sharif, and S. Mumtaz, Eur. Phys. Plus **132**, 26 (2017).

[49] M. Sharif, and S. Mumtaz, Int. J. Mod. Phys. D **26**, 1741007 (2017).

[50] A. Övgün, and I. Sakalli, Theor. Math. Phys. **190**, 120 (2017).

[51] A. Övgün, and K. Jusufi, Adv. High Energy Phys. **2017**, 1215254 (2017).

[52] A. Övgün, and I. G. Salako, Mod. Phys. Lett. A **32**, 1750119 (2917).

[53] A. Övgün, and K. Jusufi, Eur. Phys. J. Plus **132**, 543 (2017).

[54] M. Z. U. Bhatti, A. Anwar, and S. Ashraf, Mod. Phys. Lett. A **32**, 1750111 (2017).

[55] M. Z. U. Bhatti, Z. Yousaf, and S. Ashraf, Ann. Phys. **383**, 439 (2017).

[56] A. Eid, Astrophys. Space Sci. **364**, 8 (2019).

[57] A. Eid, J. Korean Phys. Soc. **70**, 436 (2017).

[58] A. Eid, New Astron. **53**, 6 (2017).

[59] A. Eid, Indian J. Phys. **91**, 1451 (2017).

[60] A. Eid, Indian J. Phys. **92**, 1065 (2018).

[61] S. Chakraborty, Gen. Relativ. Gravit. **49**, 47 (2017).

[62] S. Chakraborty, S. Dutta, and S. Chakraborty, Eur. Phys. J. Plus. **133**, 308 (2018).

[63] K. Jusufi, and A. Övgün, Mod. Phys. Lett. A **32**, 1750047 (2017).

[64] S. H. Mazharimousavi and M. Halilsoy, Int. J. Mod. Phys. D **27**, 1850028 (2018).

[65] S. H. Mazharimousavi, Z. Amirabi, and M. Halilsoy, Mod. Phys. Lett. A **32**, 1750064 (2017).

[66] S. H. Mazharimousavi, Eur. Phys. J. C **78**, 612 (2018).

[67] D. Wang, and X. H. Meng, Phys. Dark Universe **17**, 46 (2017).

[68] E. R. Celis, C. Tomasini, and C. Simeone, Int. J. Mod. Phys. D **27**, 1750171 (2018).

[69] O. Svitek, and T. Tahamtan, Eur. Phys. J. C **78**, 167 (2018).

[70] Z. Amirabi, M. Halilsoy, and S. H. Mazharimousavi, Mod. Phys. Lett. A **33**, 1850049 (2018).

[71] Z. Amirabi, Eur. Phys. J. C **79**, 410 (2019).

[72] N. Tsukamoto, and T. Kokubu, Phys. Rev. D **98**, 044026 (2019).

[73] P. K. F. Kuhfittig, Turk. J. Phys. **43**, 213 (2019).

[74] A. Khaybullina, and G. Tuleganova, Mod. Phys. Lett. A **34**, 1950006 (2019).

[75] A. C. Li, W. L. Xu, and D. F. Zeng, J. Cosmol. Astropart. Phys. **3**, 016 (2019).

[76] V. Dzhunushaliev, V. Folomeev, B. Kleihaus, and J. Kunz, Phys. Rev. D **99**, 044031 (2019).

[77] T. Bandyopadhyay, and S. Chakraborty, Class. Quantum Gravity **26**, 085005 (2009).

[78] S. H. Mazharimousavi, M. Halilsoy, and Z. Amirabi, Class. Quantum Gravity **28**, 025004 (2011).

[79] S. H. Mazharimousavi, and M. Halilsoy, Eur. Phys. J. C **75**, 81 (2015).

[80] S. H. Mazharimousavi, and M. Halilsoy, Eur. Phys. J. C **75**, 271 (2015).

[81] S. H. Mazharimousavi, and M. Halilsoy, Eur. Phys. J. C **75**, 540 (2015).

[82] M.G. Richarte, and C. Simeone, Phys. Rev. D 76, 087502 (2007); Erratum Phys. Rev. **77**, 089903 (2008).

[83] M.K. Zangeneh, F.S.N. Lobo, and M.H. Dehghani, Phys. Rev. D **92**, 124049 (2015).

[84] E. F. Eiroa, and C. Simeone, Phys. Rev. D **76**, 024021 (2007).

[85] J. P. S. Lemos, and F. S. N. Lobo, Phys. Rev. D **78**, 044030 (2008).

[86] F. S. N. Lobo, and R. Garattini, J. High Energy Phys. **1312**, 065 (2013).

[87] E. Guendelman, A. Kaganovich, E. Nissimov, and S. Pacheva, AIP Conf. Proc. **1243,** 60 (2010).

[88] S. Bahamonde, D. Benisty, and E. I. Guendelman, Universe **4**, 112 (2018).

[89] C. Hoffmann, T. Ioannidou, S. Kahlen, B. Kleihaus, and J. Kunz, Phys. Rev. D **97**, 124019 (2018).

[90] C. Hoffmann, T. Ioannidou, S. Kahlen, B. Kleihaus, and J. Kunz, Phys. Rev. D

95, 084010 (2017).

[91] C. Lanczos, Phys. Zeits **23,** 539 (1922).

[92] G. Darmois, Mémorial de Sciences Mathématiques, **25** (1927).

[93] W. Israel, Nuovo Cimento **44B**, 1 (1966).

[94] V. de la Cruz, and W. Israel, Nuovo Cimento **51A**, 774 (1967).

[95] J. E. Chase, Nuovo Cimento **67B**, 136. (1970).

[96] S. K. Blau, E. I. Guendelman, and A. H. Guth, Phys. Rev. D **35**, 1747 (1987).

[97] R. Balbinot, and E. Poisson, Phys. Rev. D **41**, 395 (1990).

[98] R. M. Wald, *General Relativity* (University of Chicago Press; UK ed. edition 2010).

[99] M. C. Bento, O. Bertolami, and A. A. Sen, Phys. Rev. D **66**, 043507 (2002).

[100] P. K. F. Kuhfittig, Acta Physica Polonica B **41**, 9, 2017 (2010).

[101] P. K. F. Kuhfittig, Adv. High Energy Phys. **2012**, 462493 (2012).

[102] P. S. Letelier, Phys. Rev. D **20**, 1294 (1978).

[103] S. G. Ghosh, U. Papnoi, and S. D. Maharaj, Phys. Rev. D **90**, 044068 (2014).

[104] M. Sharif, and S. Mumtaz, Adv. High Energy Phys. **2014**, 639759 (2014).

[105] A. Eid, Gravit. Cosmol. **24**, 378 (2018).

[106] E. F. Eiroa, and C. Simeone, Phys. Rev. D **71**, 127501 (2005).

[107] D. Garfinkle, G. T. Horowitz and A. Strominger, Phys. Rev. D **43**, 3140 (1992); Erratum Phys. Rev. D **45**, 3888 (1992).

[108] G. W. Gibbons and K. Maeda, Nucl. Phys. B **298**, 741 (1988).

[109] S. I. Vacaru, and D. Singleton, J. Math. Phys. **43**, 2486 (2002).

[110] K. A. Bronnikov, and J. P. S. Lemos, Phys. Rev. D **79,** 104019 (2009).

[111] K. A. Bronnikov, and V. G. Krechet, Int. J. of Modern Phys. D **31**, 1641022 (2012).

[112] K. A. Bronnikov, V. G. Krechet, and J. P. S. Lemos, Phys. Rev. D **87**, 084060 (2013).

[113] K. A. Bronnikov, J. Phys. Conf. Ser. **675**, 012028 (2016).

[114] S. S. Hashemi, and N. Riazi, Gen. Rel. Gravit. **48**, 130 (2016).

[115] S. S. Hashemi, and N. Riazi, Gen. Rel. Gravit. **50**, 19 (2018).

[116] A. Sepehri, T. Ghaffary, Y. Naimi, H. Ghaforyan, and M. Ebrahimzadeh, Int. J of Geom. Meth. in Mod. Phys. **15**, 1850043 (2018).

[117] E. F. Eiroa, and C. Simeone, Phys. Rev. D **82**, 084039 (2010).

[118] E. F. Eiroa, and C. Simeone, Phys. Rev. D **81**, 084022 (2010); Erratum Phys. Rev. D **90**, 089906 (2014).

[119] C. Simeone, Int. J. of Modern Phys. D **21**, 1250015 (2012).

[120] E. de Celis, O. P. Santillan, and C. Simeone, Phys. Rev. D **86**, 124009 (2012).

[121] M. G. Richarte, Phys. Rev. D **87**, 067503 (2013).

[122] M. G. Richarte, Phys. Rev. D **88**, 027507 (2013).

[123] M. Sharif, and M. Azam, Eur. Phys. J. C **73**, 2407 (2013).

[124] M. Sharif, and S. Mumtaz, Can. J. Phys. **94**, 158 (2016).

[125] M. R. Setare, and A. Sepehri, J. High Energy Phys. **03**, 079 (2015).

[126] A. Eid, Eur. Phys. J. Plus **131**, 298 (2016).

[127] M. V. Sazhin, O. S. Khovanskaya, M. Capaccioli, G. Longo, M. Paolillo, G. Covone, N. A. Grogin and E. J. Schreier, Mon. Notices Royal Astron. Soc **376**, 1731 (2007).

[128] E. Morganson, P. Marshall, T. Treu, T. Schrabback, and R. D. Blandford, Mon. Notices Royal Astron. Soc **406**, 2452 (2010).

[129] T. Vachaspati, and A. Vilenkin, Phys. Rev. Lett. **67**, 1057 (1991).

[130] M. S. Movahed, B. Javanmardi, and R. K. Sheth, Mon. Notices Royal Astron. Soc **434**, 3597 (2013).

[131] A. Vafaei Sadr, M. S. Movahed, M. Farhang, C. Ringeval, and F. R. Bouchet, Mon. Notices Royal Astron. Soc **475**, 1010 (2018).

[132] S. Aneesh, S. Bose, and S. Kar, Phys. Rev. D **97**, 124004 (2018).

[133] B. P. Abbott *et al.*, Phys. Rev. Lett. **119**, 161101 (2017).

[134] B. P. Abbott et al., Astrophys. J. **848**, 2 (2017).

[135] A. Einstein, and N. Rosen, J. Franklin Inst. **223**, 43 (1937).

[136] M. Halilsoy, Nuov. Cim. B **102**, 563 (1988).

[137] T. Levi-Civita, Rend. Acc. Lincei, **28,** 101 (1919).

[138] C. S. Trendafilova, and S. A. Fulling, Eur. J. Phys. **32,** 1663 (2011).

[139] J. P. S. Lemos, Class. Quantum Grav. **12,** 1081 (1995).

[140] M. F. A. da Silva, A. Wang, and F. M. Paiva, Phys. Rev. D **61,** 044003 (2000).

[141] M. Zofka, and J. Bičák, Class. Quantum Grav **25,** 015011 (2008).

[142] I. Brito, M. F. A. Da Silva, F. C. Mena, and N. O. Santos, Gen Relativ Gravit **46,** 1681 (2014).

[143] E. F. Eiroa, and C. Simeone, Phys. Rev. D **91,** 064005 (2015).

[144] B. Linet, J. Math. Phys. (N.Y.) **27,** 1817 (1986).

[145] Q. Tian, Phys. Rev. D **33,** 3549 (1986).

[146] W. B. Bonnor, Class. Quantum Grav **25,** 225005 (2008).

[147] V. Perlick, Living Rev. Relativity **7,** 9 (2004).

[148] J. R. Gott, Astrophys. J. **288,** 422 (1985).

[149] M. van de Meent, Phys. Rev. D **87**, 025020 (2013).

[150] T. Kibble, J. Phys. A **9**, 1387 (1976).

[151] E. F. Eiroa, E. R. de Celis, and C. Simeone, Eur. Phys. J. C **76,** 546 (2016).

[152] J. P. S. Lemos, and V. T. Zanchin, Phys. Rev. D **54**, 3840 (1996).

[153] V. Cardoso, and J. P. S. Lemos, Class. Quantum Grav. **18** 5257 (2001).

[154] J. D. Brown, and J. W. York Jr., Phys. Rev. D **47,** 1407 (1993).

[155] S. Mertens, J. Phys.: Conf. Ser. **718,** 022013 (2016).

[156] K. Hinterbichler, Rev. Mod. Phys. **84**, 671 (2012).

[157] C. de Rham, Living Rev. Relativ. **17**, 7 (2014).

[158] M. Fierz, and W. Pauli, Proc. Roy. Soc. Lond. A **173**, 211 (1939).

[159] B. Gavela, E. E. Jenkins, A. V. Manohar, and L. Merlo, Eur. Phys. J. C **76**, 485

(2016).

[160] S. Deser, R. Jackiw, and S. Templeton, Ann. Phys. **140**, 372 (1982); **185**, 406(E) (1988).

[161] S. Deser, R. Jackiw, and S. Templeton, Ann. Phys. **281**, 409 (2000).

[162] E. A. Bergshoeff, O. Hohm, and P. K. Townsend, Phys. Rev. Lett. **102**, 201301 (2009).

[163] E. A. Bergshoeff, O. Hohm, and P. K. Townsend, Phys. Rev. D **79**, 124042 (2009).

[164] E. A. Bergshoeff, O. Hohm, and P. K. Townsend, J. Phys. Conf. Ser. **229,** 012005 (2010).

[165] I. Oda, J. High Energy Phys. **05**, 064 (2009).

[166] M. Nakasone, and I. Oda, Prog. Theor. Phys. **121**, 6 (2009).

[167] K. Muneyuki, and N. Ohta, Phys. Rev. D **85**, 101501(R) (2012).

[168] C. de Rham, G. Gabadadze, D. Pirtskhalava, A. J. Tolley, and I. Yavin, J. High Energy Phys. **06,** 028 (2011).

[169] A. Accioly, J. Helayël-Neto, E. Scatena *et al.*, Class. Quantum Grav. **28**, 225008 (2011).

[170] A. Accioly, J. Helayël-Neto, J. Morais *et al.*, Phys. Rev. D **83**, 104005 (2011).

[171] G. Clement, Class. Quantum Grav. **26**, 105015 (2009).

[172] M. Bañados, C. Teitelboim, and J. Zanelli, Phys. Rev. Lett. **69**, 1849 (1992).

[173] G. Clement, Class. Quantum Grav. **26**, 165002 (2009).

[174] E. Ayon-Beato, G. Giribet and M. Hassaine, J. High Energy Phys. **05,** 029 (2009).

[175] J. Oliva, D. Tempoa, and R. Troncoso, J. High Energy Phys. **07,** 011 (2009).

[176] E. Ayón-Beato, A. Garbarz, G. Giribet, and M. Hassaine, Phys. Rev. D **80**, 104029 (2009).

[177] H. Ahmedov, and A. N. Aliev, Phys. Rev. Lett. **106**, 021301 (2011).

[178] H. Ahmedov, and A. N. Aliev, Phys. Rev. D **83**, 084032 (2011).

[179] H. Ahmedov, and A. N. Aliev, Phys. Lett. B **694**, 143 (2010).

[180] Y. S. Myung, Y. W. Kim, T. Moon *et al.*, Phys. Rev. D **84**, 024044 (2011).

[181] J.M. Maldacena, Adv. Theor. Math. Phys. **2,** 231 (1998); Int. J. Theor. Phys. **38**, 1113 (1999).

[182] Y. Liu, and Y. W. Sun, J. High Energy Phys. **04**, 106 (2009).

[183] D. Grumiller, and O. Hohm, Phys. Lett. B **686**, 264 (2010).

[184] M. R. Setare, and V. Kamali, Adv. High Energy Phys. 472718 (2011).

[185] M. Eune, W. Kim, S.-H. Yi, J. High Energy Phys. **1303**, 020 (2013).

[186] Y. S. Myung, Adv. High Energy Phys. **2015**, 478273 (2015).

[187] S. J. Zhang, Phys. Lett. B **747**, 158 (2015).

[188] Y. Kwon, S. Nam, J. D. Park, and S. H. Yi, Class. Quantum Grav. **28,** 145006 (2011).

[189] G. Gecim, and Y. Sucu, J. Cosmol. Astropart. Phys. **02**, 023 (2013).

[190] E. Bergshoeff, J. J. Fernandez-Melgarejo, J. Rosseel, and P. K. Townsend, J. High Energy Phys. **04**, 070 (2012).

[191] D. Dalmazi, and R. C. Santos, Phys. Rev. D **87**, 085021 (2013).

[192] I. Güllü, T. C. Şişman, and B. Tekin, Class. Quantum Grav. **27**, 162001 (2010).

[193] I. Güllü, T. C. Şişman, and B. Tekin, Phys. Rev. D **82**, 024032 (2010).

[194] A. Ghodsi, and D. Mahdavian Yekta, Phys. Rev. D **83**, 104004 (2011).

[195] A. Sinha, J. High Energy Phys. **06**, 061 (2010).

[196] S. Nam, J.-D. Park, and S.-H. Yi, J. High Energy Phys. **07**, 058 (2010).

[197] G. G. Anastasiou, M. R. Setare, and E. C. Vagenas, Phys. Rev. D **88**, 064054 (2013).

[198] M. R. Setare, and M. Sahraee, Int. J. Mod. Phys. A **28**, 14 (2013).

[199] D. Dalmazi, and E. L. Mendonca, Eur. Phys. J. C **76**, 373 (2016).

[200] H. Ahmedov, and A. N. Aliev, Phys. Lett. B **711**, 117 (2012).

[201] H. L. C. Louzada, U. Camara dS, and G. M. Sotkov, Phys. Lett. B **686**, 268 (2010).

[202] U. Camara dS, and G. M. Sotkov, Phys. Lett. B **694**, 94 (2010).

[203] A. Ghodsi, and M. Moghadassi, Phys. Lett. B **695**, 359 (2011).

[204] I. Bakas, and C. Sourdis, Class. Quantum Grav. **28**, 015012, (2011).

[205] A. Akhavan, M. Alishahiha, A. Naseh *et al.*, J. High Energy Phys. **05**, 006 (2016).

[206] T. Dereli, and C. Yetişmişoğlu, EPL **114**, 60004 (2016).

[207] T. Dereli, and C. Yetişmişoğlu, Phys. Rev. D **94**, 064067 (2016).

[208] N. Deruelle, M. Sasaki, and Y. Sendouda, Prog. Theor. Phys. **119**, 237 (2008).

[209] B. Reina, J. M. M. Senovilla, and R. Vera, Class. Quantum Grav. **33**, 105008 (2016).

[210] E. F. Eiroa, G. F. Aguirre, and J. M. M. Senovilla, Phys. Rev. D **95**, 124021(2017).

[211] E. F. Eiroa, and G. F. Aguirre, Eur. Phys. J. C **78**, 54 (2018).

[212] J. Y. Kim, C. O. Lee, and M. Park, Eur. Phys. J. C **78**, 990 (2018).

[213] S. D. Forghani, S. H. Mazharimousavi, and M. Halilsoy, Eur. Phys. J. C **78**, 469 (2018).

[214] S. D. Forghani, S. H. Mazharimousavi, and M. Halilsoy, Eur. Phys. J. Plus **134**, 342 (2019).

[215] S. D. Forghani, S. H. Mazharimousavi, and M. Halilsoy, Eur. Phys. J. C **79**, 449 (2019).

[216] S. D. Forghani, S. H. Mazharimousavi, and M. Halilsoy, Eur. Phys. J. Plus **133**, 497 (2018).

[217] S. D. Forghani, S. H. Mazharimousavi, and M. Halilsoy, doi.org/10.1142/S0218271819501426 (2019).

[218] S. D. Forghani, S. H. Mazharimousavi, and M. Halilsoy, arxiv: 1807.05080 (2018).